Title
The Aerodynamic Forces On Misaligned Platoons

Permalink

Authors
Marcu, Bogdan
Browand, Fred

Publication Date
1998

The Aerodynamic Forces on Misaligned Platoons

Bogdan Marcu, Fred Browand
University of Southern California

The contents of this report reflect the views of the authors who are responsible for the facts and the accuracy of the data presented herein. The contents do not necessarily reflect the official views or policies of the State of California. This report does not constitute a standard, specification, or regulation.

The Aerodynamic Forces on Misaligned Platoons (MOU 245)

by

Bogdan Marcu
Fred Browand

Department of Aerospace Engineering
University of Southern California
Los Angeles, California, 90089-1191

Executive Summary

This report summarizes wind tunnel experimental measurementson the aerodynamic interaction between members of misaligned platoons. Experiments are conducted at the University of Southern California's Dryden Wind Tunnel Facility.

All experiments are made using 1/8 scale models of 1991 Chevy Lumina minivan. Models are placed above a ground plane with a porous surface, through which slight suction is applied to remove the boundary layer. Refurbishing of the ground plane surface, and its repositioning to a 1 degree angle of attack produce significantly improved air flow through the test section. Automatization of the testing procedures allow measurements of drag, side force and yawing moment with extremely fine position resolution. The measured quantities are presented in the form of coefficient ratios by *ratioing* the forces and moment with the value of drag experienced by a vehicle in isolation.

The results of two separate experiments are presented in this report. First, aerodynamic forces on misaligned three-vehicle platoons are presented for all possible platoon configurations resulting from a longitudinal separation range of 0 to 0.72 vehicle lengths and a lateral displacement range of 0 to 1.1 vehicle widths for the middle vehicle. Results are presented in the form of color maps of the drag, side force and yawing moment coefficient ratios for each individual vehicle in the platoon. Experimental results from a complete set of symmetric configurations and five sets of non-symmetric configurations, associated with five fixed separations between the leading vehicle and the trailing vehicle, are presented in detail.

A second experiment consists of a detailed investigation of aerodynamic forces on a two-vehicle platoon in *back-to-back* geometry. Following previous observations, the present experiment investigates a two-fold increase in drag force occurring at specific separations between the two vehicles. Color maps for the drag, side force and yawing moment coefficient ratios document the presence of a hysteresis loop–the drag on the leading vehicle as separation increases is different from drag as separation narrows. It is argued that the resonance with hysteresis represents a matching between the wavelength of turbulent flow structure and the spacing itself. A dimensional analysis relates the drag increase phenomenon to longitudinal separations between different types of vehicles.

I. Overview

The concept of Automated Highway Systems includes, among other highway traffic strategies, the idea of close-following, which imagines platoons of vehicles equipped with computer controlled braking, steering and throttle as well as speed and position sensors, traveling at speeds of the order of 60 to 80 mph at spacings significantly smaller than one vehicle length. The potential of this idea is basically a three-fold (J. Rillings 1997) in the traffic flow on a typical freeway, with consequent fuel and time savings, as well as reduced quantities of engine emissions.

When vehicles are perfectly aligned in a platoon traveling at close spacing, they interact aerodynamically to the benefit of all members of the platoon. The drag reduction experienced by each vehicle in a platoon was documented in a series of wind tunnel experiments (Zabat et al. 1995) which predicted that a two-vehicle platoon would have an average drag coefficient of roughly 75% the value associated with a single vehicle in isolation, while an eight-vehicle platoon would have an average drag coefficient of approximately half the value associated with a single vehicle in isolation. All vehicles in the platoon, including the lead vehicle experience the drag reduction (Browand et al. 1997). Recent field test results (Hong et al. 1997) confirmed the wind tunnel results for two close-following vehicles.

Nevertheless, while important drag savings occur when vehicles are perfectly aligned in a platoon, situations arise in practice when the vehicles are misaligned. When platoons are formed, or when one member of an n-vehicles platoon reaches a destination and must therefore exit the platoon, the alignment of the vehicles is broken, as the vehicle joining or leaving the platoon moves laterally. The question arises as to how the process of aerodynamic interaction between the vehicles may be affected by the misalignment. Furthermore, the detachment of one vehicle from the platoon is a complex operation from the point of view of the control systems guiding this operation. Communications between vehicles and a change in the control protocols for certain vehicles in the platoon occur simultaneously. The vehicle behind the one exiting the platoon becomes a temporary platoon leader as the vehicle leaving the platoon is automatically steered out to an adjoining lane. From this standpoint, a second question may arise as to how the changes in the aerodynamics affect the stability of the control systems, and what type of precautions must be taken in oder to avoid dangerous situations. In order to address these problems, one needs accurate knowledge of the detailed aerodynamic interactions between the vehicles in a misaligned platoon.

The present report contains a synthesis of results obtained from an extensive set of wind tunnel experiments–comprising 200 hours of wind tunnel testing–addressing the aerodynamic interaction between the members of a three-vehicle platoon when the middle vehicle is moved laterally, from the aligned position to a displacement of approximately one vehicle width. The experiments are carried at the University of Southern California's Dryden Wind Tunnel Facility, using 1/8 scale models of the 1991 Chevy Lumina minivan. Each model is equipped with a force balance (presented in detail in Zabat et al. 1993) able to measure the aerodynamic drag, side force and yawing moment. The models are mounted above a porous ground plane surface and slight suction is applied to control the boundary layer.

This report also contains a second set of measurements conducted with two model vehicles placed

back-to-back. For this particular geometry, the drag of the leading vehicle can change by a factor of two as spacing changes by only a few percent of the vehicle length. Similar but less dramatic variations in drag occur in other multi-vehicle configurations, but we choose to study this extreme case in detail.

The remainder of the report is organized as follows. Chapter II contains a discussion of the experimental method, and updates our earlier wind tunnel methods. Chapter III contains results and discussion of the three vehicle misaligned platoon. Chapter IV contains results and discussion of the back-to-back geometry. In a brief Chapter V, describe the work to be achieved during the coming two years.

A set of 9 databases is provided along with this report. The databases contain the values of aerodynamic forces on each member of a three-vehicle platoon, for all geometrical configurations investigated. The raw data acquired during experiments, the data acquisition programs, and the Matlab data processing programs require a large volume of disk storage and it is not included here but it can be provided upon request on a CD-ROM.

II. Experimental Method

1. Measurements and associated corrections

Previous reports (Zabat et al. 1993, 1995) have established the necessary confidence in the wind tunnel results obtained at the University of Southern California's Dryden Wind Tunnel Facility.

The three quantities measured on each vehicle during the previous and present experiments are:

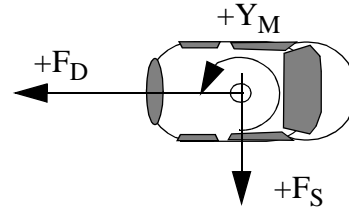- the drag force: F_D
- the side force: F_S
- the yawing momentum: Y_M

Figure 1.a. Convention of signs for the drag force F_D, side force F_S and yawing momentum Y_M.

Special force balances have been designed and build at USC for measuring these quantities. A detailed description of the force balance is given in the report by Zabat et al. 1993. The convention of signs for forces are shown in figure 1.a. Figure 1.b shows the configuration of a misaligned three-vehicle platoon, with equal, symmetric longitudinal spacing between the vehicles s_1. Misalignment of a vehicle s_2 is defined as the lateral offset from the platoon centerplane to the centerplane of the misaligned vehicle.
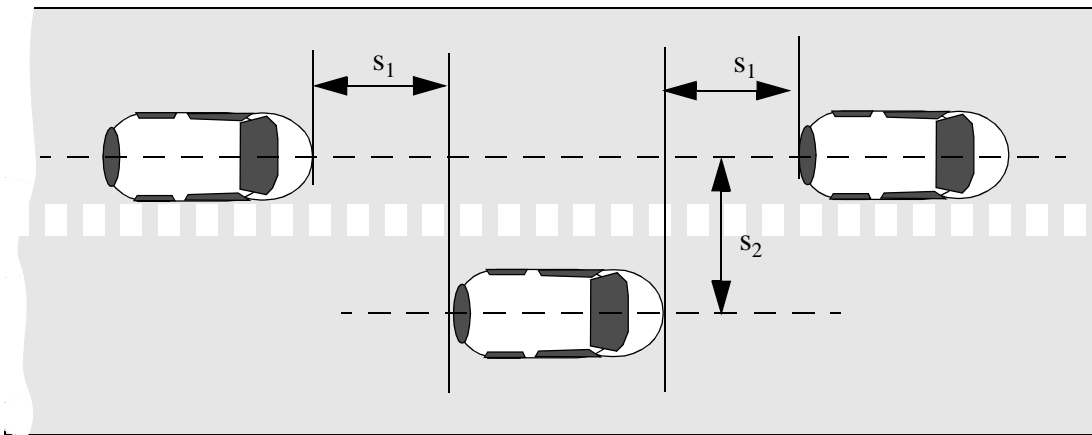

Figure 1.b. Misaligned platoon configuration.

Since the experiments presented in this report use 1/8 scale models, special care is taken to establish conditions consistent with aerodynamic phenomena experienced by full scale vehicles. However, as stated in earlier reports, perfect similarity with the real flow around the full scale vehicle is never achieved in practice, for several reasons:

i) Matching the Reynolds number for a full scale vehicle, where

$$Re = \frac{Ud}{\nu}$$

is defined by the vehicle forward speed U, a characteristic length scale d and the kinematic viscosity of the air ν, would require wind tunnel speeds 8 times higher that the road speed to account for the characteristic length d which is 8 times smaller for a vehicle model. This, of course, is not possible, and while an automobile driving at highway speed may correspond to $Re = O(10^6 - 10^7)$, the wind tunnel tests are conducted at a Reynolds number about one order of magnitude lower.

ii) The presence of the wind tunnel walls destroys the geometric similarity with the real free-way situation where the flow-field in not bounded.

iii) In real life, the vehicle moves relative to the road, but in the wind tunnel vehicle and road are stationary in the airstream. The ground plane in the wind tunnel develops a boundary layer which does not exist on the roadway.

Certain corrections can be made in order to render the wind tunnel results much closer to reality. Each of the aspects presented above is dealt with either by arranging the measured quantities in a special form, or by applying carefully crafted correction procedures:

i) By defining dimensionless force coefficients rather than using raw force values, one can automatically account for differences in vehicle size and vehicle speed. A drag coefficient is defined as

$$C_D = \frac{F_D}{\frac{1}{2}\rho U A}$$

where ρ is the air density, A is the maximum cross-sectional area of the body, perpendicular to the flow, and U is the wind tunnel air speed relative to the vehicle. Similarly, a side force coefficient and a yawing moment coefficient are defined as

$$C_S = \frac{F_S}{\frac{1}{2}\rho U A}$$

$$C_Y = \frac{Y_M}{\frac{1}{2}\rho U A^{\frac{3}{2}}}$$

ii) A special correction procedure is applied to account for the presence of the wind tunnel walls. The procedure is presented in detail in the report by Zabat et al. 1993. A static pressure distribution $p = p(x)$ is measured along the ceiling of the test section while the tunnel is running, first when the tunnel is empty, and then when the a model or a set of

5

models in a platoon formation are mounted in the tunnel. A pressure difference coefficient is calculated as

$$\Delta C_p(x) = (p_{empty} - p_{model})/(1/2\rho U_\infty^2)$$

Here ρ is again the air density, and U_∞ is the wind tunnel air speed at the front of the test section, where the presence of the model does not affect the local static pressure. Locating the position x_{max} where maximum in the pressure difference coefficient ΔC_p is recorded, a correction coefficient is defined as

$$C_w = \frac{1}{1 - C_p(x_{max})}$$

where $C_p(x_{max}) = (p_\infty - p(x_{max}))/(1/2\rho U_\infty^2)$, p_∞ is the static air pressure measured at the front of the tunnel test section where the presence of the model does not affect the air flow, and $p(x_{max})$ is the static air pressure measured at the x_{max} location with the model(s) mounted in the wind tunnel. Correcting the drag coefficient C_D with the wall correction coefficient C_W accounts approximately for the presence of the walls in the wind tunnel.

iii) Control of the boundary layer is achieved by applying uniform suction to the entire ground plane which is constructed with a porous upper surface allowing for the removal of the low speed fluid in the boundary layer. The procedure is described in detail in the next section.

In addition, the measured quantities are always *ratioed* with the corresponding quantities for a vehicle in isolation. Repeated measurements are made using a single vehicle model, placed at the exact location in the wind tunnel corresponding to its position in the platoon. For each vehicle the values of the forces measured in isolation–corrected and rendered dimensionless in the form of force coefficients–are then used to compute a *ratio* between the value of the force coefficients obtained from measurements in platoon configuration and the values corresponding to the same vehicle in isolation.

$$\hat{C}_D = \frac{C_D}{C_{D\infty}} \quad \hat{C}_S = \frac{C_S}{C_{D\infty}} \quad \hat{C}_Y = \frac{C_Y}{C_{D\infty}}$$

 Using all these additional procedures, the effects of any uncertainties due to non-similarities between the wind tunnel flow regime and the flow regime around the full-sized vehicles are considerably diminished.

2. Treatment of the boundary layer

A detailed description of the porous ground plane used for the present experiments is given in the report by Zabat et al. 1993. The ground plane actually consists of a hollow, box-like structure 5.8

meters in length, 1.30 meters in width and 10 cm in thickness. The upper surface is constructed with interchangeable, perforated steel plates. The downstream end of the ground plane box contains a sheet metal suction duct. The duct exits on both sides of the test section underneath the ground plane, and connects the plenum to two AVR 90-75 D1298 axial fans that provide the necessary pressure drop to remove the boundary layer air from the ground plane surface.

Initially, the evenly distributed hole pattern in the porous upper surface was designed with 7% open area. The previous experiments were carried out using 3.74 mm Hg suction (Zabat et al. 1995). An ideal suction should remove the ground plane boundary layer and provide a pressure coefficient in the empty tunnel

$$C_p(x) = \frac{p_\infty - p(x)}{\frac{1}{2}\rho U_\infty^2}$$

as small in absolute value and as close to being constant along the wind tunnel test section as possible. Practically, boundary layer growth on the other test section walls, where suction is not applied, creates a slightly increasing air velocity and a decreasing $C_p(x)$.

The ground plane was refurbished for the present experiments by applying a Clear Focus® coating of plastic porous material uniformly over the entire surface of the plate, thus reducing the open area to an estimate of 4%. Furthermore, the ground plane box was mounted in the wind tunnel with an angle of attack of 1°, in order to compensate for boundary layer growth on the lateral and upper walls. The upper half of the test section (above the ground plane) and lower half (below the ground plane box) were carefully sealed in order to prevent leakage . The result of these refurbishing details on the quality of the flow is shown is
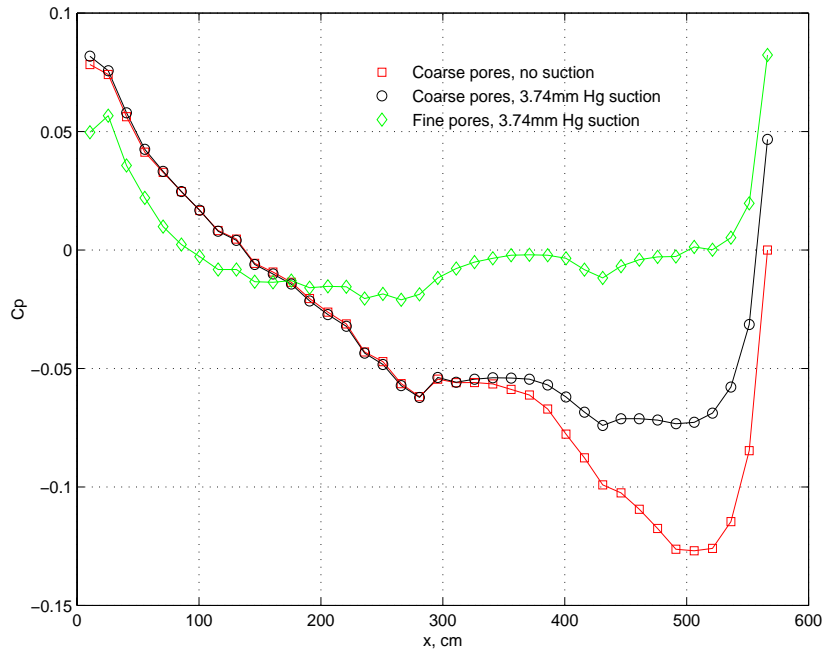
Figure 2. Pressure coefficient distributions along the wind tunnel test section

Figure 2. The coarse porous $C_p(x)$ distribution corresponds to the initial design of 7% open area of the ground plane. Shown are the $C_p(x)$ distribution with and without suction. The fine porous $C_p(x)$ distribution corresponds the refurbished ground plane, when 3.74 mm Hg suction is applied. The new angle of attack setting of the ground plane has removed the steep linear gradient between zero and 2.5 meters downstream. What remains is an almost flat pressure distribution extending from x = 0.75 meters to x = 5.0 meters.

3. Experimental set-up and procedures for misaligned three-vehicle platoon tests

Vehicle Positioning System. A computer controlled positioning system for the vehicle models has been designed and mounted within the ground plane box. The models are mounted on carriages which travel along optical rails mounted on the bottom wall of the ground plane box. The leading and trailing vehicle of the three-vehicle platoon are allowed to move longitudinally along the wind tunnel axis to achieve different vehicle spacing configurations, while the middle vehicle moves laterally to achieve different degrees of misalignment. The position of each

Figure 3.

model-vehicle can be precisely varied using a stepper motor interfaced with the computer. The stepper motors are driven by an Anaheim Automation® BL6-3 driver. The BL6-3 driver is interfaced with a MacIntosh® Quadra™ 950 computer via a National Instruments® NB-DIO-24 digital I/O board. Limit switches prevent the carriages from reaching the Unislide stops on both ends of the travel, thus preventing damages to the driving thread.

Figure 4.

The limit switches are also used to reset the models to a reference position after each test. For all three drives, the stepper motor drives the screw of a VELMEX® Unislide™ at a rate of 200 steps per rotation allowing an accurate positioning within ±0.05 milimeters from a desired position. A matrix of platoon configurations can easily be programmed and produced during the experiment. Figure 3 is a photograph the ground plane box, with the porous panels removed on one side, showing the stepper motor which controls the middle vehicle lateral position and the carriage on which the middle vehicle is mounted. Also shown is the carriage supporting the leading vehicle. The mounts which support the upper porous panels can also be observed in the figure. Figure 4 shows the ground plane box with all porous panels mounted, and the three-vehicle platoon in a configuration of 0.5 vehicle lengths spacing and 1.0 vehicle widths lateral displacement. The slots observed in the picture allow access for the rods supporting the vehicles. The slots are covered with Clear Focus® porous plastic material during the experiment in order to avoid suction non-uniformities.

Instrumentation and Data Acquisition. Each vehicle model is equipped with a force balance designed and fabricated at USC. Zabat (Zabat et al. 1993) gives a detailed description of the design, and calibration procedures for the force balance. The force balance is mounted on the underside of each vehicle model, with its center positioned at 0.535 ±0.003 vehicle lengths behind the front bumper (vehicle length is 0.616 m). The yawing moment as shown in figure 1.a is referenced to this central point. Each force balance is interfaced with the Quadra™ 950 computer via a National Instruments® NB-MIO-16H-9 multifunction I/O board containing a 12-bit ADC (±10 V max) with a maximum sampling rate of 100 Ksamples/sec.

The test section wind speed is measured using a Pitot-static tube of 0.32 cm diameter. A static pressure rail approximately 5.80 meters in length and containing 38 static pressure taps at 15.2 cm spacings is fixed along the center line of the tunnel ceiling. A thermocouple, fixed to the tunnel wall is used to monitor the air temperature in the wind tunnel. All pressure measurements are made using two MKS® Baratron™ 310CD pressure sensors paired with a 270B signal conditioner/readout. Accuracy of this system is 0.1% of the full scale (10 mm Hg). A Scanivalve™ is used to step from one pressure port to another. The outputs from the two 270B signal conditioners are also read into the computer through the NB-MIO-16H-9 multifunction I/O board.

Test Procedures. All platoon configurations, corresponding to a vehicle spacing range $0.0 \le s_1 \le 0.72$ (in vehicle lengths) and a misalignment range of $0.0 \le s_2 \le 1.1$ (in vehicle widths), are investigated. To accomplish this, a configuration matrix of 30 longitudinal positions for the leading vehicle, 30 longitudinal positions for the trailing vehicle and 14 lateral positions for the middle vehicle is programmed into the computer. The coordinates of these positions are denser for configurations corresponding to short spacing and small misalignment in order to capture variations in forces for small configuration changes with appropriate resolution. The total of 12,600 configurations is divided into 30 sub-matrices, each comprising a separate run. During a run, 12 signals (four voltages for each of the three force balances) are acquired and digitized at a rate of 1024 digitizations per second. Force and moment values are defined by 8 second data averages. Each run lasts 6 hours and 38 minutes, accounting for a total of approximately 200 hours of testing. All three models are re-calibrated after each run.

After testing all platoon configurations, measurements are made for each model in isolation, for each position that specific model had in every platoon configuration. These measurements provide the reference C_D values referred to as C_{Dref} or $C_{D\infty}$. The static pressure distribution in the test section is read at nodes of a configuration matrix comprising 10 longitudinal vehicle spacings and 4 lateral displacements and allows an accurate interpolation for intermediate configurations.

The matrix of all test configurations is geometrically presented in the form of a pyramid in figure 5. The base of the pyramid corresponds to the largest longitudinal vehicle spacing while the top corresponds to zero spacing. The lateral dimension of the pyramid is constant throughout its height, corresponding to the lateral middle vehicle displacement for each longitudinal vehicle spacing investigated. All possible positions of the leading vehicle are measured along the centerplane of the front face (face A) of the pyramid, and all possible positions of the trail vehicle are measured along the centerplane of the back face (face B) of the pyramid. The position of the middle vehicle is measured by moving laterally along the apex of the pyramid. The configuration data set represents all possible combinations of these three coordinates. Since it is difficult to present

results in four dimensions–orce plus three coordinates–we adopt the following scheme. First, coefficient ratios are presented for *symmetric longitudinal vehicle spacing*.That is, the leading and trailing vehicles ar always equally distanced about the *longitudinal* position of the middle vehicle. This corresponds to placing the central vehicle somewhere in the vertical plane labeled "plane of symmetric spacing", while the leading and trailing vehicle positions are restricted to the front and back faces of the pyramid. This way, the central plane labeled "plane of symmetric spacing" becomes a two-dimensional domain whose vertical coordinate corresponds to a certain longitudinal spacing while the lateral coordinate corresponds to a certain misalignment. A second, *non-symmetric* mapping of data corresponds to choosing five horizontal planes in figure 2.5, each of which represent *fixed total separation* between leading and trailing vehicles. The misaligned vehicle is free to move on this horizontal plane–one such plane is labeled "plane of non-symmetric vehicle spacing" in the figure. These abbreviations reduce the dimensionality of the data set to three dimensions. Force and moment coefficient ratios for each of the three vehicles are plotted separately. A series of final plots give drag coefficient ratios averaged over all three vehicles for both the symmetric and non-symmetric cases.
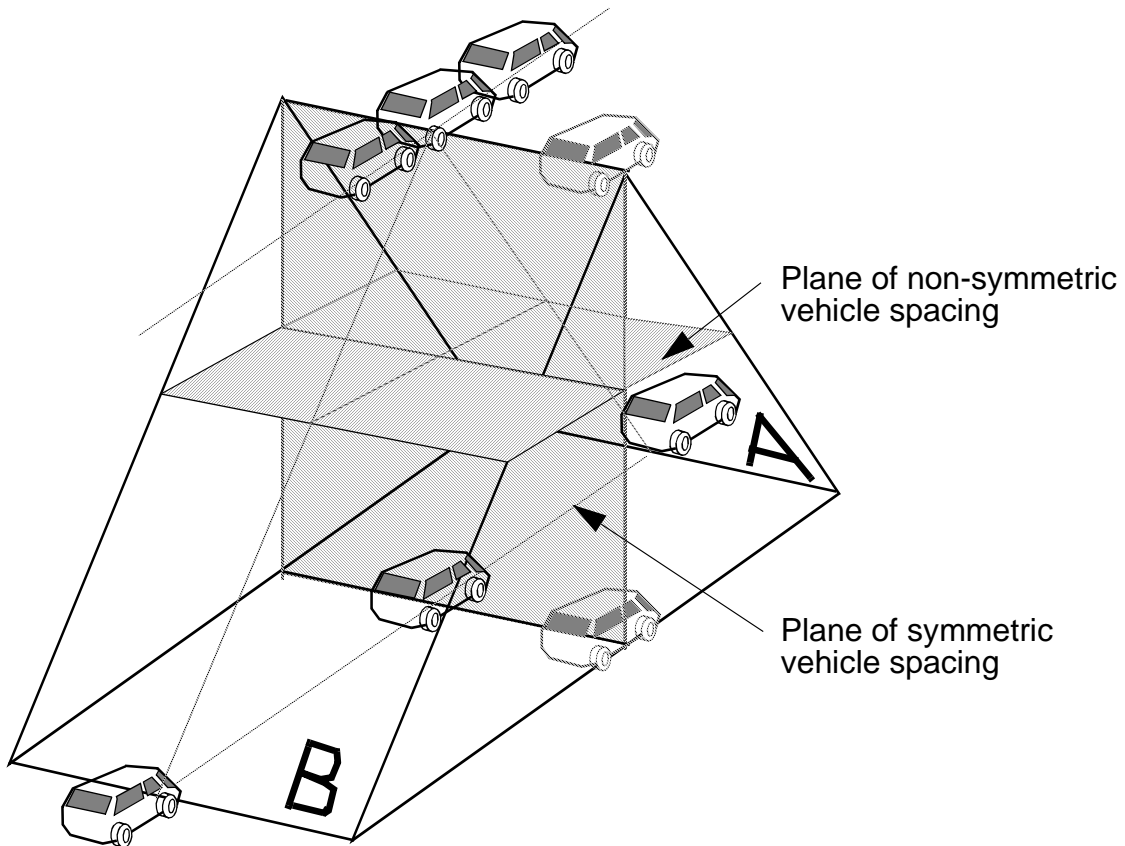
Figure 5. The platoon configurations pyramid. The top of the pyramid corresponds to zero longitudinal spacing, while the base corresponds to maximum longitudinal spacing.

III. Quasi-Steady Forces On Misaligned Three-Vehicle Platoons

1. The role of quasi-steady misalignment

In the present study, misalignment is defined as the lateral offset between the centerplane of the platoon and the centerplane of the misaligned vehicle. The misalignment is produced by moving only the middle vehicle laterally. After the vehicle reaches its desired position, the drag, side force and yawing moment are measured and recorded. Such a measurement represents a *quasi-steady force limit*, in the sense that sufficient time has been given for the flow field to sense and respond to the altered vehicle arrangement. The time required for flow adjustment is a transit time–typically the time for a parcel of fluid to traverse the flow field. In the platoon case, this time might be the time to travel a distance of a vehicle length. For vehicles traveling at 60 mph (97 Km/hr), the flow time is of the order of 200 milliseconds. Vehicle movements taking place on time scales shorter than the flow time scale are inherently *unsteady*, and must be modeled by unsteady movements. Vehicle movements taking place on time scales comparable to, or greater than the flow time can be approximated as *quasi-steady*. The quasi-steady limit is always an important base to establish, and from which to judge unsteady flow forces.

2. Aerodynamic forces on misaligned platoons at symmetric longitudinal vehicle spacing.

Drag, side force and yawing momentum are measured for a complete set of platoon configurations with symmetric longitudinal spacing between the members of the platoon. As shown in figure 5. all configurations with symmetric spacing correspond to the center vertical plane drawn in the figure. The quantities measured are rendered dimensionless, corrected and ratioed with the values obtained for a vehicle in isolation, as described in Section II. Results are presented in the forms of color maps for the force coefficient ratios

$$\hat{C}_D = \hat{C}_D(s_1, s_2) \qquad \hat{C}_S = \hat{C}_S(s_1, s_2) \qquad \hat{C}_Y = \hat{C}_Y(s_1, s_2)$$

where s_1 and s_2 are the longitudinal vehicle spacing and lateral misalignment. of the middle vehicle, expressed in vehicle lengths and vehicle widths correspondingly.

In figure 6, colormaps for the drag coefficient ratio are shown for the a) lead, b) middle and c) trailing vehicles. A colorscale is plotted along each map to help the reader translate colors into values, however, the colorscale is uniquely defined for all three maps: dark blue corresponds to lowest drag values measured for all of the platoon members, while intense red corresponds to highest drag value recorded. Also note that the vertical axis of the maps runs from zero spacing at the bottom side of the map–corresponding to the tip of the configurations pyramid, to maximum of 0.72 vehicle lengths spacing in the upper side of each map–corresponding to the base of the configurations pyramid.

For all three members of the platoon, misalignment up to ±0.2 vehicle widths do not produce any significant change from the drag in the aligned configuration. For larger misalignment, however, the situation changes, and each member of the platoon displays different effects. Drag variations for the lead vehicle are observed for misalignment larger than ±0.2 vehicle widths and spacings from zero to 0.3 vehicle length. For spacings larger than 0.3 vehicle lengths, the leading vehicle

becomes more insensitive to misalignment, as demonstrated by contour lines with a horizontal trend. The middle vehicle is the most sensitive to misalignment effect, as might be expected. At spacings of approximately 0.05 vehicle lengths, drag coefficient ratio values vary from around 0.45 (perfectly aligned situation) to 0.8-0.85 as soon as misalignment is larger than ±0.2 vehicle widths. At increased spacing, a low drag regime extends to ±0.35 vehicle widths misalignment. For misalignments larger than ±0.4 vehicle widths, the middle vehicle experiences significant changes in drag with increasing misalignment, as indicated by the dense contour lines aligned vertically. Remarkably, the middle vehicle still experiences some 5-10% reduction in drag, for misalignments of about ±0.8 vehicle widths and spacing of 0.7 vehicle lengths. However, at misalignments of ±1.0-1.1 vehicle widths, drag force on the middle vehicle equals and slightly exceeds the drag experienced in isolation. It is when the vehicle is almost out of the platoon that the situation is the most unfavorable. Furthermore, the *change* in drag coefficient ratio from around 0.7 to 1-1.06 occurs over a short range of misalignment values–a difference of around 0.6 vehicle widths.

The trailing vehicle appears to be the least sensitive to misalignment. From zero to 0.4 vehicle lengths spacing, the changes in drag are small over the entire range of misalignment values. There is a certain degree of sensitivity for increased spacing, where misalignments larger than ±0.35 vehicle widths produce more significant changes in drag. However, the C_D values under such misalignment do not exceed 0.85.

In figure 7, colormaps of the side force coefficient ratio are shown for the a) leading vehicle, b) middle vehicle, and c) the trailing vehicle. Side force coefficient ratios $\hat{C}_S$ are expressed in fractions of drag coefficient experienced by the vehicle in isolation, thus allowing an estimation of the intensity of the side force relative to the undisturbed drag. All three maps from figure 7 reveal strong aerodynamic interaction between the vehicles of the platoon at close spacing. The largest side force values recorded occur at spacings of 0.1 vehicle lengths and smaller. The leading vehicle experiences relatively small side force values (±0.1) at misalignment smaller than 0.4-0.5 vehicle widths. At misalignments larger than 0.8 vehicle widths, and when spacing is shorter than 0.1 vehicle lengths, side forces of 0.3 to 0.4 drag fractions in magnitude develop on the leading vehicle. The largest side forces occur therefore at largest misalignment, when the middle vehicle is almost out of the platoon.   Furthermore, a change in side force of approximately 75% occurs for a change in misalignment from 0.7 to 1.1 vehicle widths. This effect diminishes when longitudinal separation increases, and for spacings larger than 0.2 vehicle lengths the side forces on the lead vehicle do not exceed 0.15 drag fractions.

The middle vehicle also experiences peak side forces at spacings shorter than 0.1 vehicle lengths, as a result of its interaction with the leading and trailing vehicles. At spacings smaller than 0.1 vehicle lengths one can observe intense side forces (0.2 to 0.4 drag fractions in magnitude) between the platoon center plane and a misalignment of ±0.4 vehicle widths. These forces are stabilizing, in the sense that they tend to bring the middle vehicle back to alignment. However, for misalignment larger than ±0.65vehicle widths, the situation is reversed: side forces of around 0.35 drag fractions in magnitude tend to push the vehicle farther from the centerplane. As spacing between vehicles increases, the observed side forces significantly decrease such that at vehicle spacings larger than 0.1 vehicle lengths, the side forces on the middle vehicle do not exceed 0.2 drag fractions in absolute value. These weaker side forces are stabilizing, in that they tend to bring

a) Leading vehicle
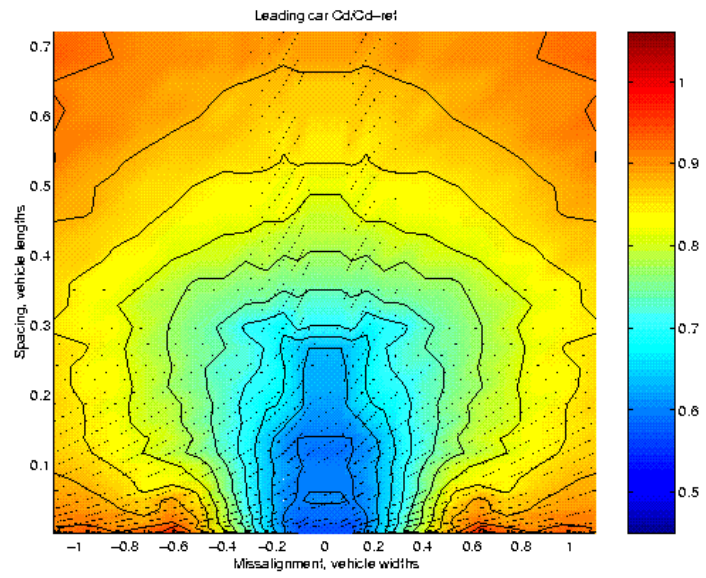
b) Middle vehicle
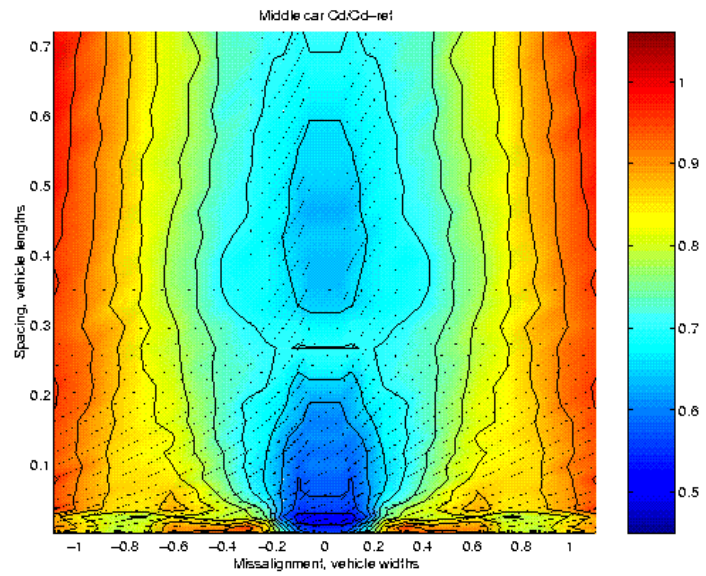
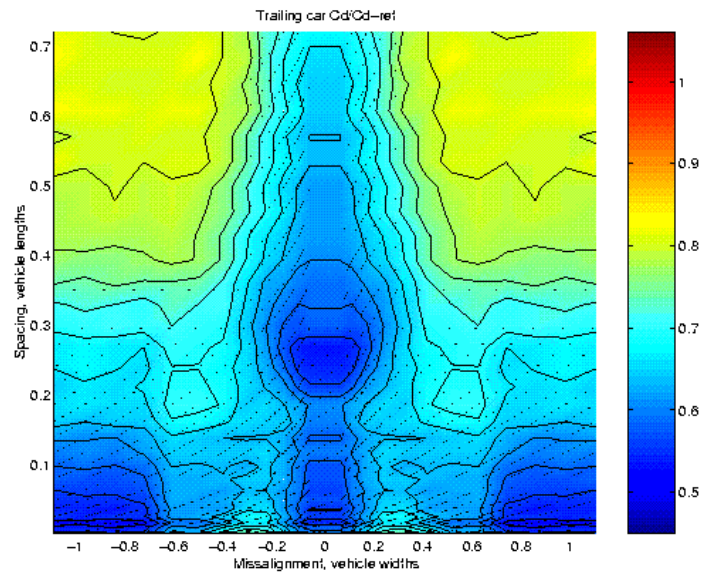**c)** Trailing vehicle

Figure 6. Drag coefficient ratio color maps for symmetric vehicle spacing in the platoon.


13

the vehicle back to alignment.

For the trailing vehicle, the most interesting effects are also observed at spacing shorter than 0.1 vehicle lengths. Side force gradients and magnitudes are weaker than for the leading and middle vehicle. At spacings up to 0.1 vehicle lengths, and for misalignment between 0.2 to 0.4 vehicle widths, side forces on the order of 0.25-0.3 drag fractions tend to pull the vehicle laterally as if to follow the misaligned vehicle. At misalignments larger than 0.5 vehicle widths, the side forces do not exceed 0.1 drag fractions. As spacing between vehicles increase to values larger than 0.2 vehicle lengths, weak side forces of the order of 0.15 drag fractions appear to be acting towards the platoon centerline - for misalignment between 0.1 to 0.4 vehicle widths- and away from the platoon centerline for misalignment larger than 0.4 vehicle widths.

Figure 8 shows colormaps of the yawing moment coefficient ratios for the a) leading vehicle, b) middle vehicle, and c) trailing vehicle. Yawing moment is expressed in terms of ratios between the yawing moment coefficient and the drag coefficient and for each vehicle the yawing moment is taken about a point 0.535 lengths behind the front bumper along the centerplane of the vehicle.

While the leading and trailing vehicle experience low yawing moment (coefficient ratios smaller than 0.03 in magnitude), interesting variations can be observed on the middle vehicle. Over the entire range of longitudinal spacings yawing moment shows similar variation: as misalignment increases, the moment increases to values of about 0.03 drag fractions, decreases to a minimum of about zero, located at around ±0.6 vehicle widths misalignment, then increases to peak values of 0.11 drag fractions at largest misalignment. The values observed at maximum misalignment at the sides of the map decrease with increased spacing. However, an interesting effect which appears in the form of "waves" on the colormap can be observed. At longitudinal spacings of 0.08, 0.12 and 0.3 vehicle lengths, peaks of high yawing moment coefficient ratio align horizontally for a misalignment range of ±0.4 to maximum misalignment. The authors believe that these peaks observed for short ranges of longitudinal spacings are a result of an aerodynamic interaction of resonant nature. A similar, but stronger effect of such interaction is discussed in Chapter IV for a separate experiment, a two-vehicle platoon in back-to-back geometric configuration.

a) Leading vehicle
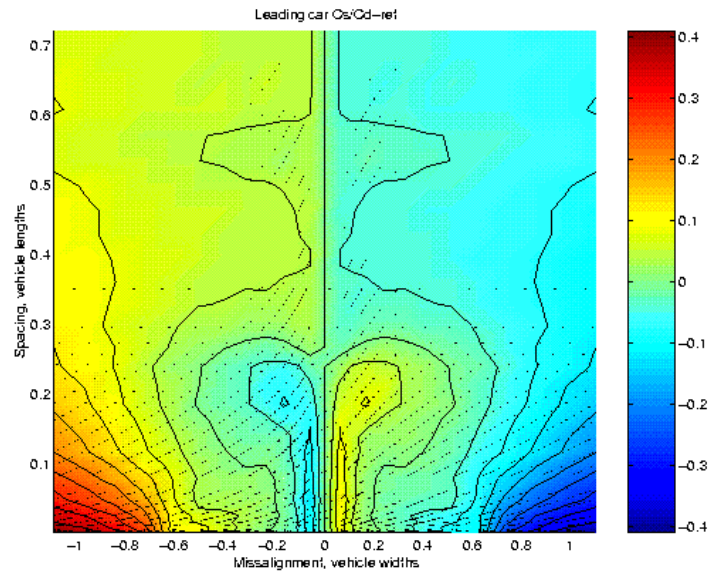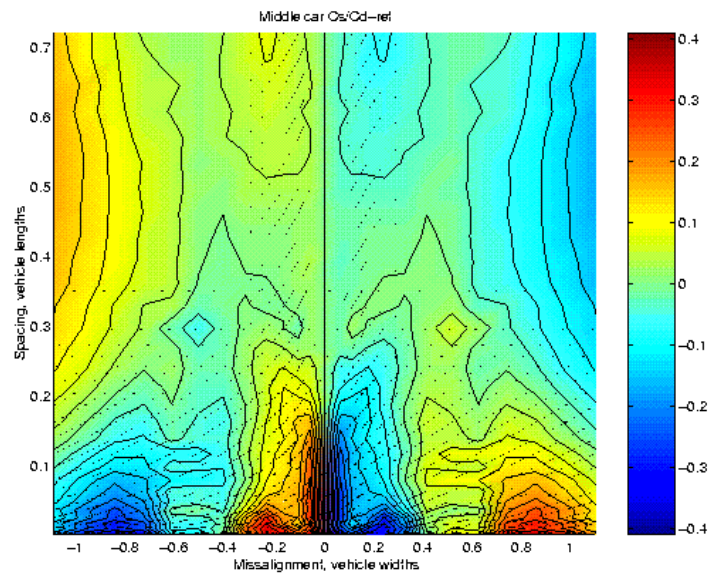
b) Middle vehicle
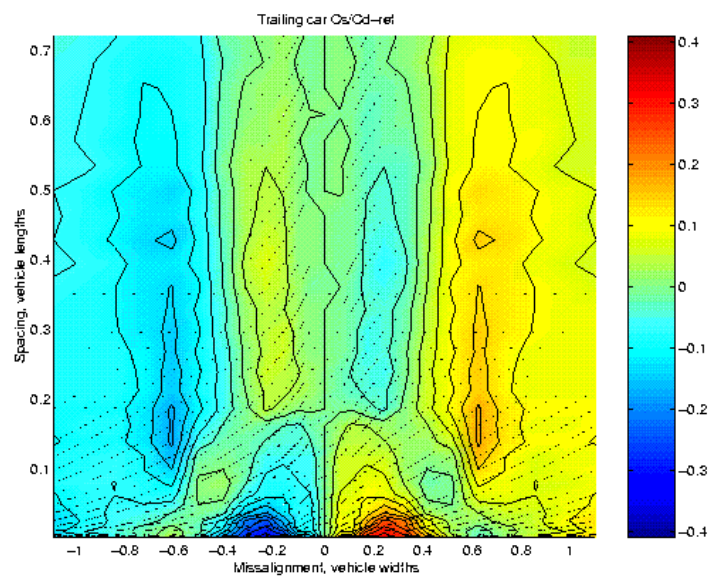
c) Trailing vehicle

Figure 7. Side force coefficient ratio color maps for symmetric vehicle spacing in the platoon.

15

a) Leading vehicle
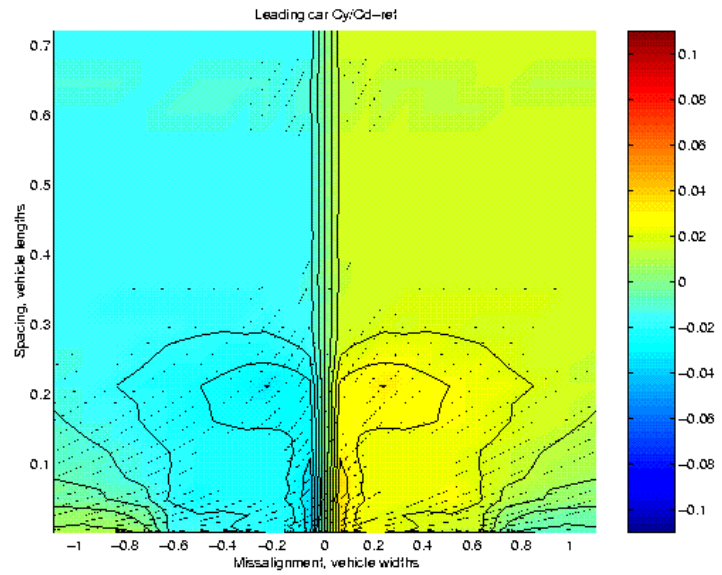
b) Middle vehicle
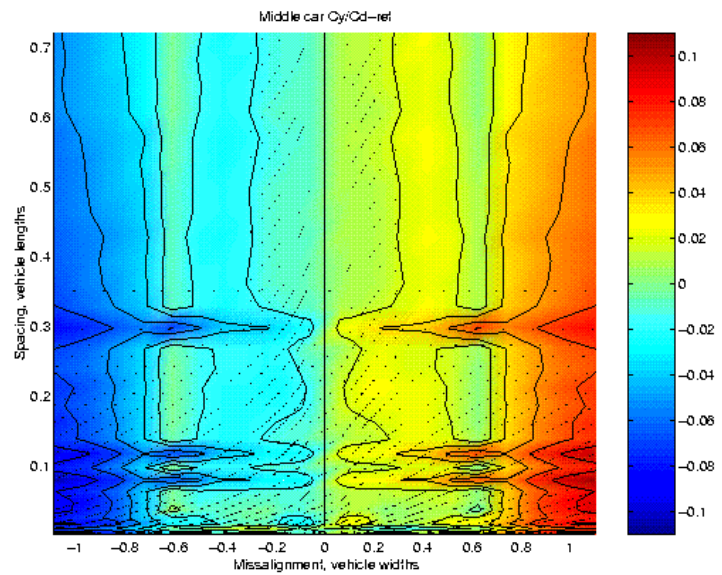
c) Trailing vehicle
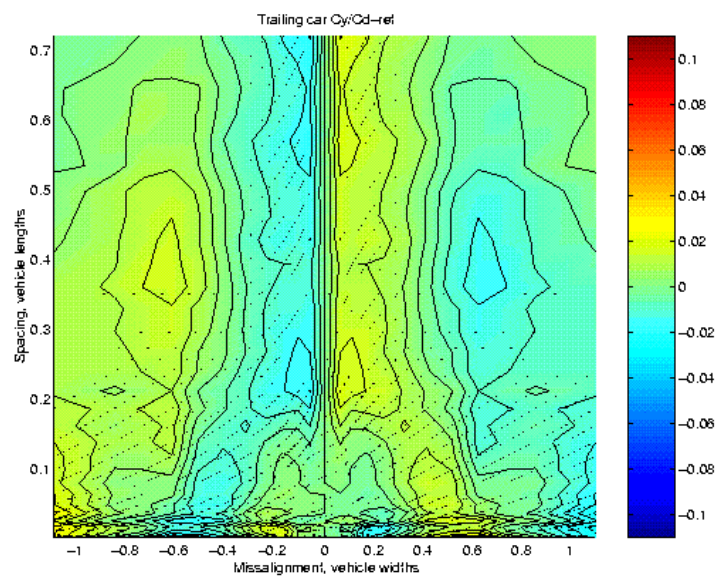
Figure 8. Yawing moment coefficient ratio color maps for symmetric vehicle spacing in the platoon.

3. The effect of non-symmetric spacing.

Misalignment in a platoon can occur while the longitudinal spacing between the vehicles is not symmetric. For example, in a multiple-vehicle platoon, while a vehicle steers out of the alignment, the spacing between that vehicle and the one ahead of it may be different than the spacing between the vehicle and the one behind.
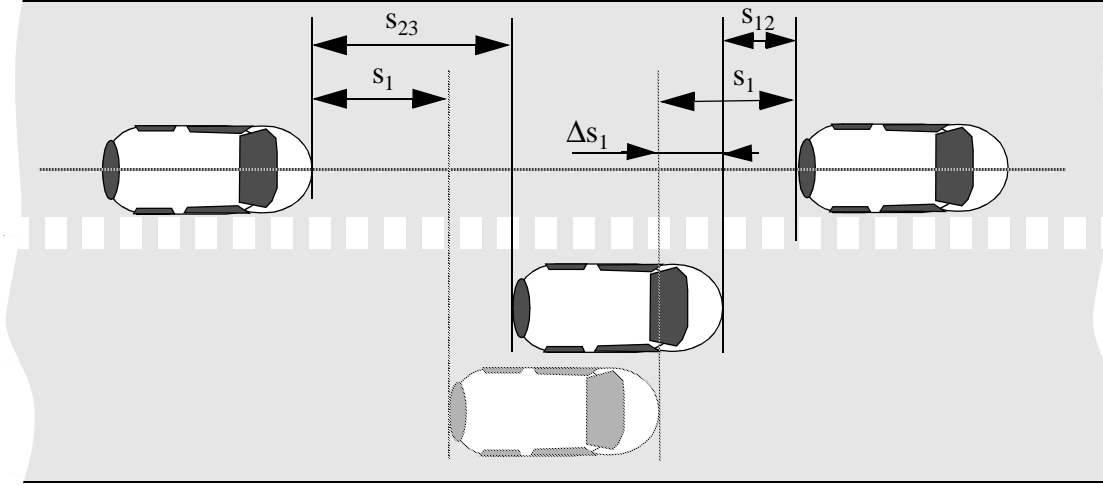
Figure 9. Non-symmetric platoon configuration

The situation is depicted in figure 9 for a three-vehicle platoon. In this sketch, s_{12} and s_{23} denote the spacing between the lead vehicle and the middle vehicle, and the spacing between the middle vehicle and the trailing vehicle, respectively. For comparison, a symmetric configuration is drawn in dotted contour, with s_1 denoting the equal (symmetric) spacing. The longitudinal displacement Δs_1 places the middle vehicle closer to the leading vehicle than in the symmetric configuration. A set of non-symmetric configurations can be generated around each symmetric configuration corresponding to a certain longitudinal spacing s_1. The spacing between the leading vehicle and the trailing vehicle is maintained constant while the longitudinal displacement Δs_1 and lateral misalignment s_2 are varied. In this manner, all non-symmetric configurations around the symmetric configuration corresponding to that specific s_1 value are investigated. Such a set corresponds to a horizontal cut through the configuration pyramid shown in figure.5. The results are presented in the form of colormaps for the force coefficient ratios

$$\hat{C}_D = \hat{C}_D(\delta s_1, s_2) \qquad \hat{C}_S = \hat{C}_S(\delta s_1, s_2) \qquad \hat{C}_Y = \hat{C}_Y(\delta s_1, s_2)$$

where $\delta s_1 = (\Delta s_1)/(2 s_1)$ is the longitudinal displacement from the symmetric s_1 spacing rendered non-dimensional, and s_2 is the misalignment of the middle vehicle. Note that δs_1 coordinate varies from -0.5 (when the spacing between the middle vehicle and trailing vehicle is zero, while the spacing between the leading and middle vehicles is maximum for the specific s_1 considered) to +0.5 (when the situation is the opposite).

Non-symmetric platoon configurations are investigated around the symmetric configurations corresponding to longitudinal spacings of 0.1, 0.21, 0.36, 0.53 and 0.72 vehicle lengths.

17

Coefficient ratios for drag, side force and yawing moment for a longitudinal spacing of 0.1 vehicle lengths are shown in figures 10, 11 and 12 respectively. Shown are colormaps whose lateral coordinate corresponds to misalignment s_2 and vertical coordinate corresponds to longitudinal displacement δs_1. One could imagine these maps being plotted on a horizontal plane cut through the configurations pyramid at a height corresponding to the spacing s_1. As one can observe in the three figures, the non-symmetry effect is small at this spacing. Only, the middle vehicle experiences some significant drag increase at misalignment around $\pm$ 0.6 vehicle widths, when longitudinal displacement is lower than -0.3 (middle vehicle closer to trailing vehicle).

The effects of non-symmetric spacing for a longitudinal spacing of 0.21 vehicle lengths is shown in figures 13 (drag coefficient ratios), 14(side force coefficient ratios) and 15 (yawing moment coefficient ratios). The drag coefficient ratios maps in figure 13.a (leading vehicle) and 13.b (middle vehicle) show that closer spacing between the leading and middle vehicles produces a reduction in drag for middle vehicle over a wide range of misalignments while narrowing the misalignment range where drag saving are observed for the leading vehicle. An opposite configuration (middle vehicle closer to the trailing vehicle) produces opposite effects: the middle vehicle becomes more sensitive to misalignment as its drag increases rapidly with increasing misalignment, while the leading vehicle experiences drag savings over a wider range of misalignments. Side force coefficient maps (figure 14) show similar effects; when the middle vehicle is closer to the leading vehicle, the situation is favorable for the middle vehicle and unfavorable for the leading vehicle. When the middle vehicle is closer to the trailing vehicle, it is the leading vehicle which experiences lower side forces while the middle vehicle experiences larger side forces. The yawing moment coefficient values show no significant change with non-symmetry in longitudinal spacing. The C_Y map for the middle vehicle (figure 15.b) displays horizontal "waves" similar to the ones observed at symmetric spacing. The trailing vehicle is not affected by non-symmetry at this longitudinal spacing.

Figures 16, 17 and 18 show the drag, side force and yawing moment coefficient ratios for non-symmetric configurations at longitudinal spacing of 0.36 vehicle lengths. One can observe again the opposite effect experienced by the leading and middle vehicles in drag force: closer spacing between leading and middle vehicles favors the middle vehicle at the expense of the leading vehicle, while closer spacing between middle and trailing vehicles favors the leading vehicle at the cost of increased sensitivity to misalignment for the middle vehicle. The trailing vehicle is not affected by non-symmetry. The largest side forces are observed on the leading vehicle when the spacing between the leading and middle vehicle is shortest. Except for the horizontal "waves" observed for the middle vehicle, yawing moment coefficient ratios are not significantly affected by non-symmetry.

A similar discussion can be provided for non-symmetric configurations corresponding to 0.53 longitudinal spacing, based on the plots shown in figures 19 (drag), 20 (side force), and 21 (yawing moment). In addition to the trends observed at smaller longitudinal spacings, some drag effects can be observed on the trailing vehicle when the middle vehicle is closer to the trailing vehicle: modest increase in drag on the trailing vehicle are observed at misalignment larger than 0.6 vehicle widths. The same configuration produces stronger values in side force (0.4 drag fractions) on the leading vehicle.

a) Leading Car

Lead Car Cd/Cd-ref
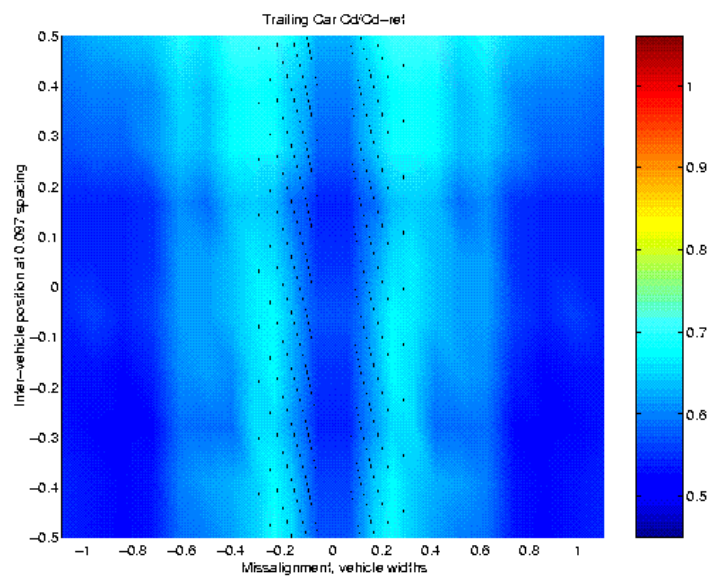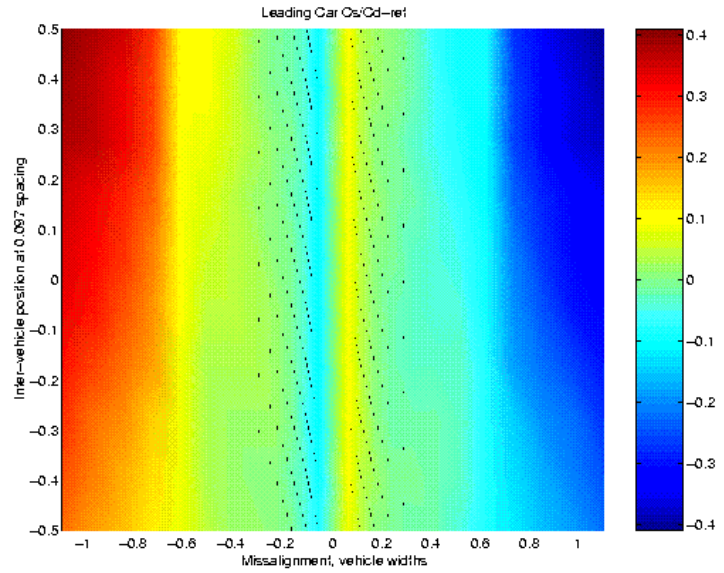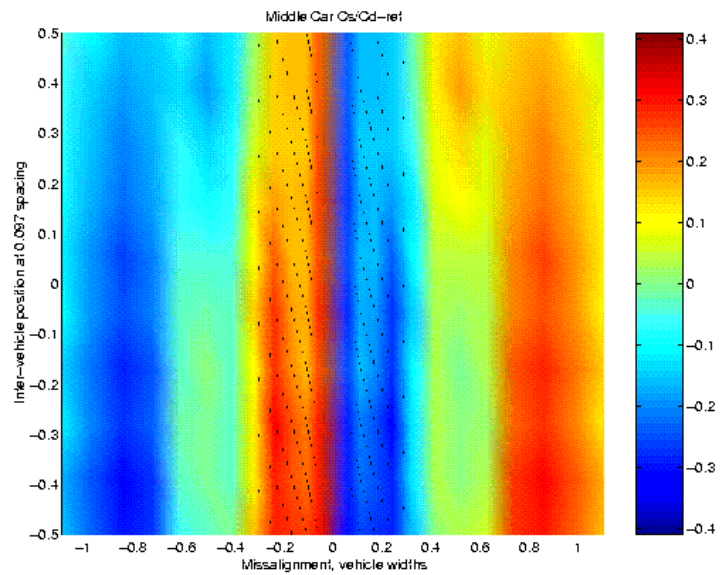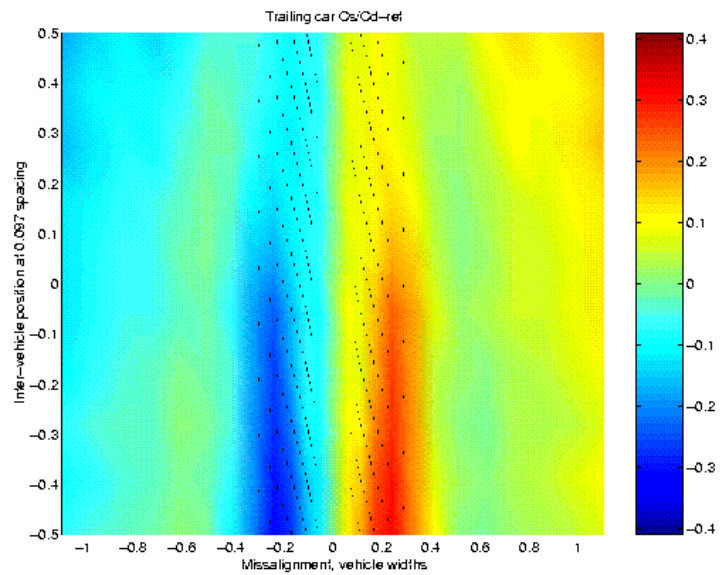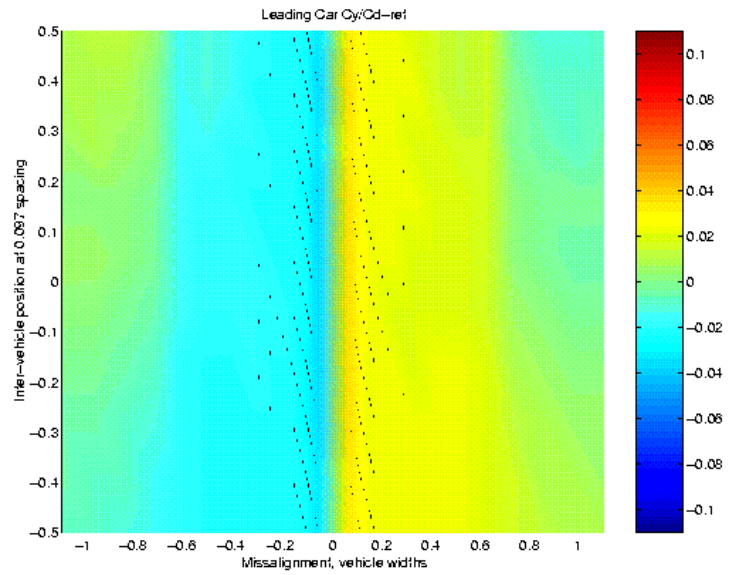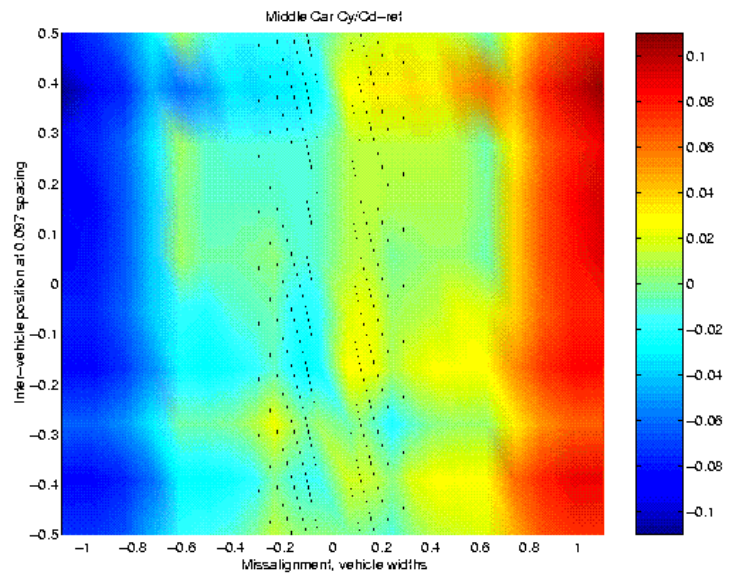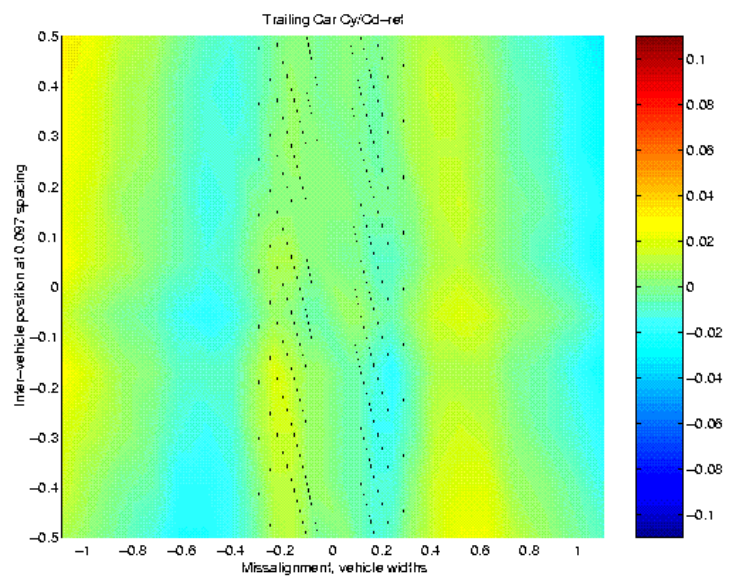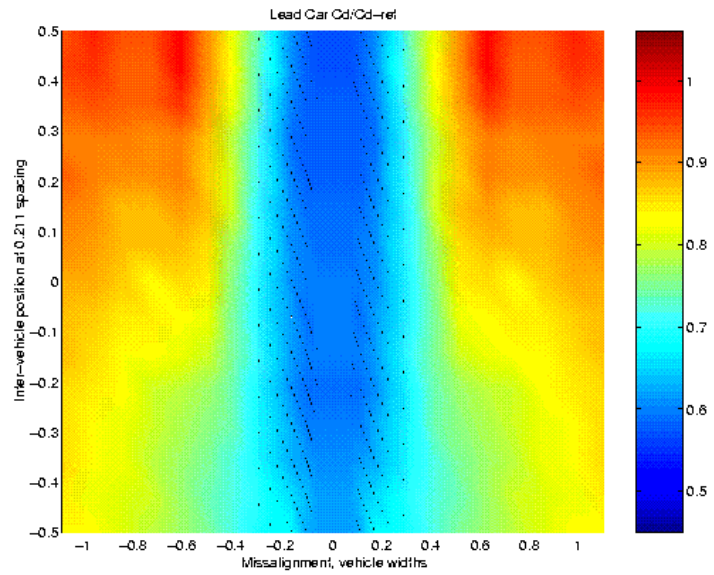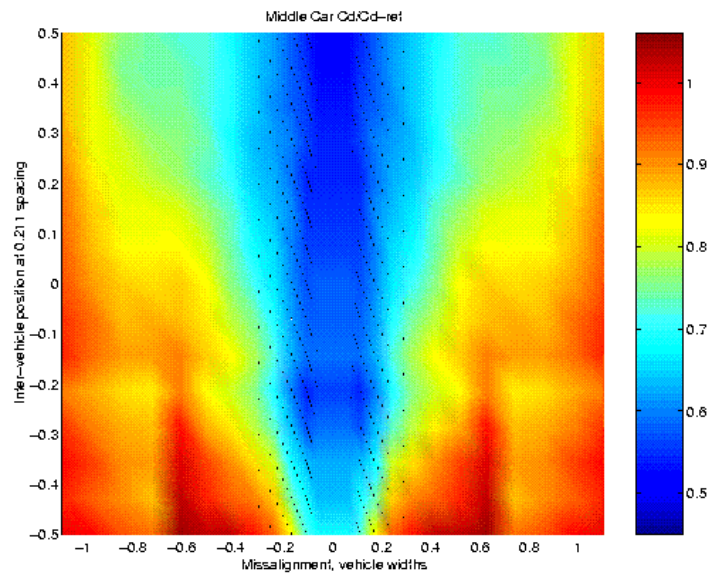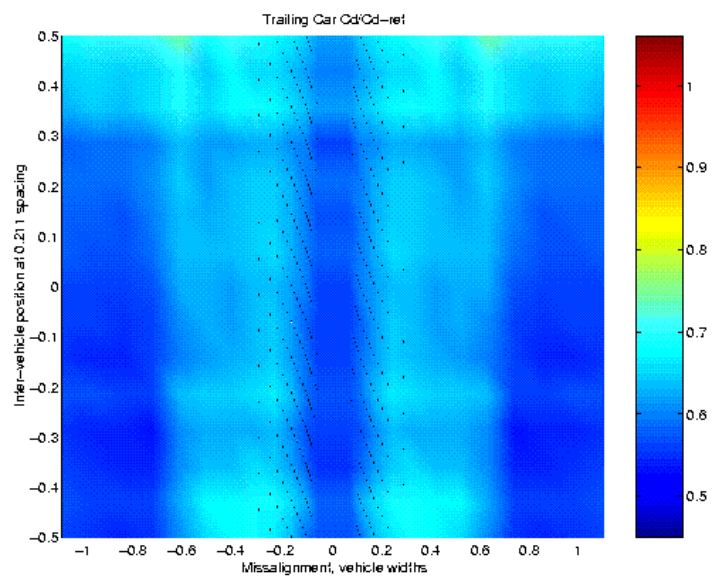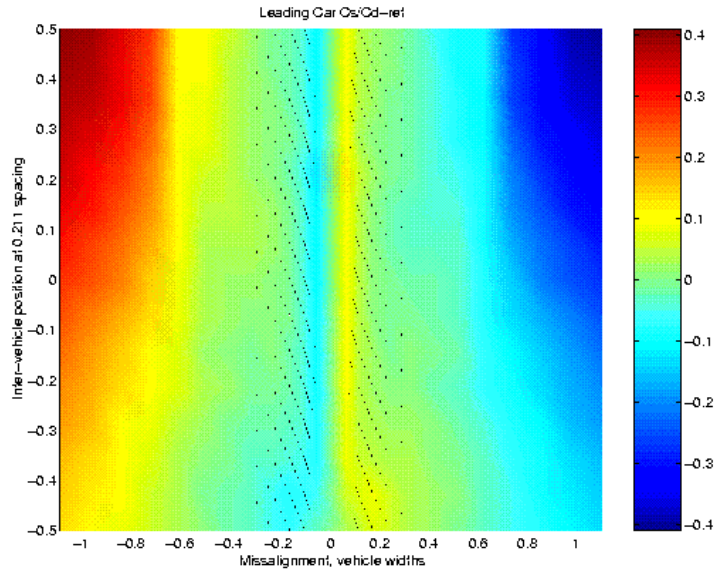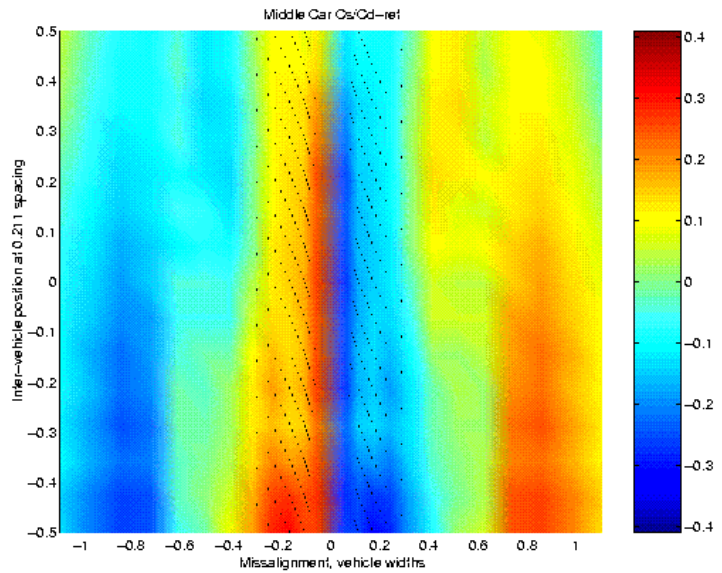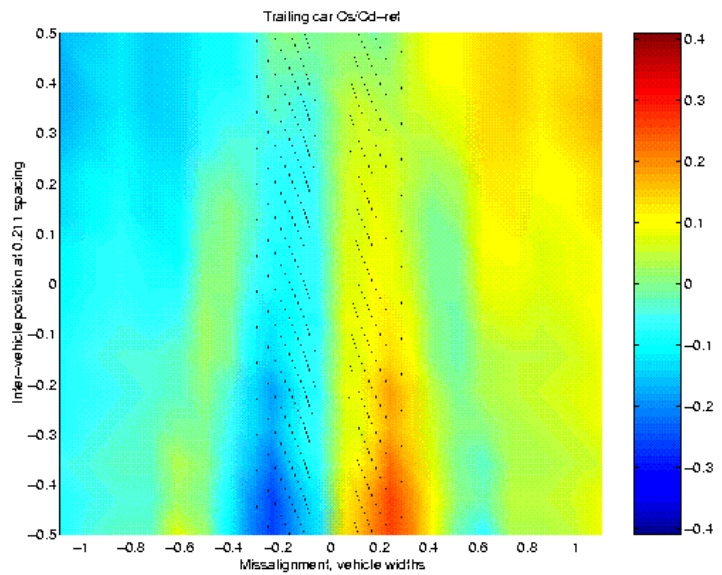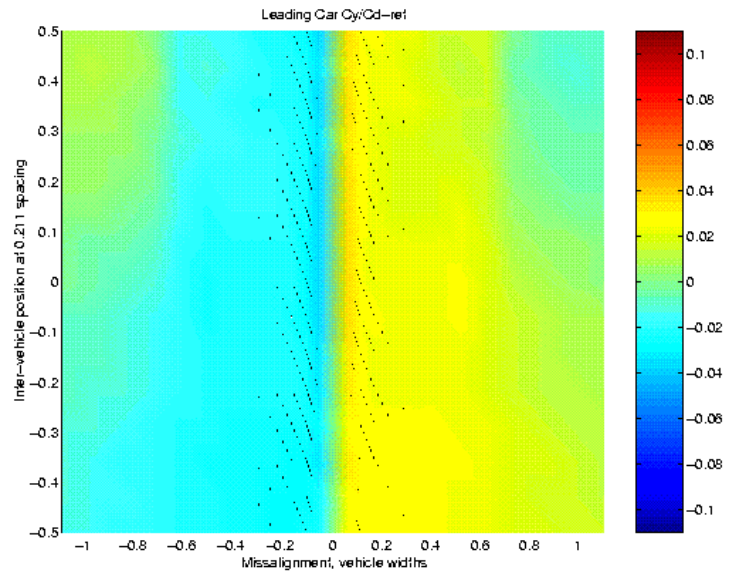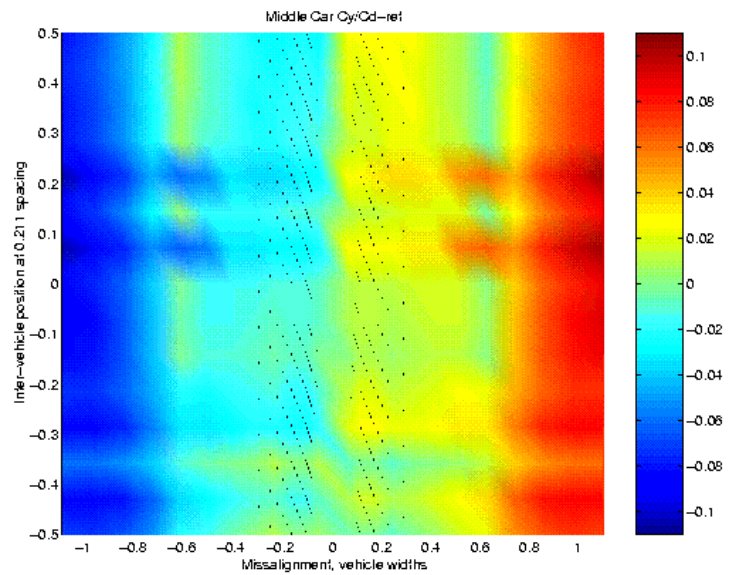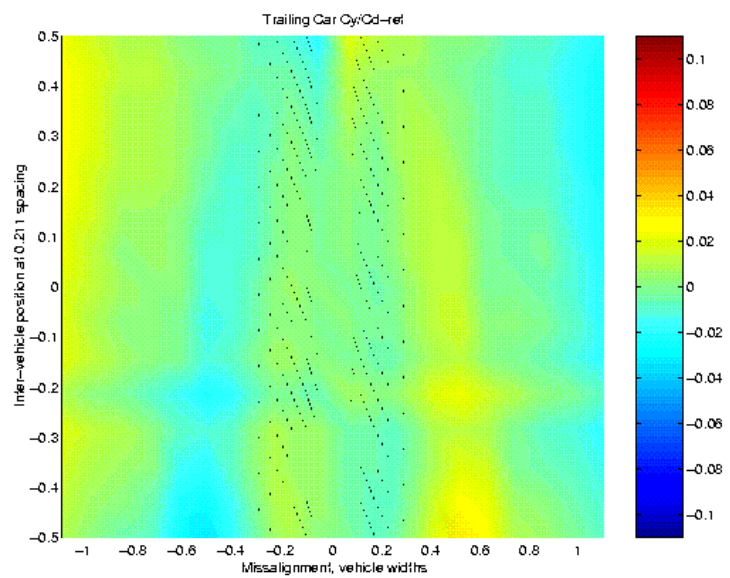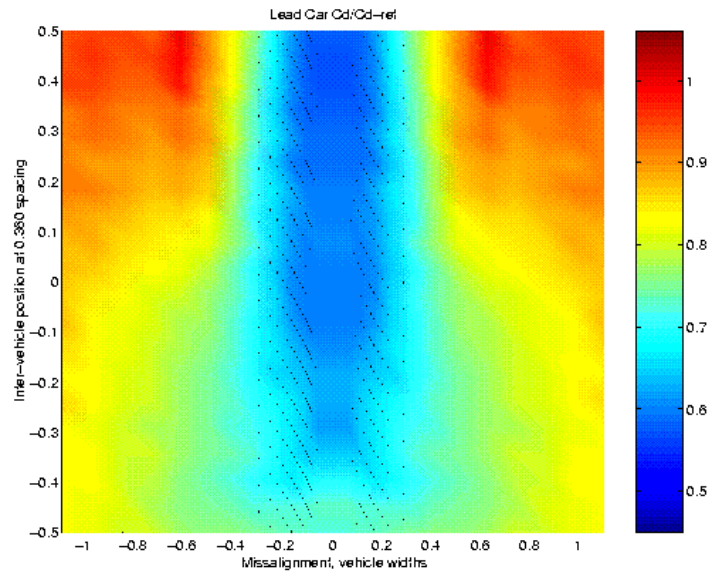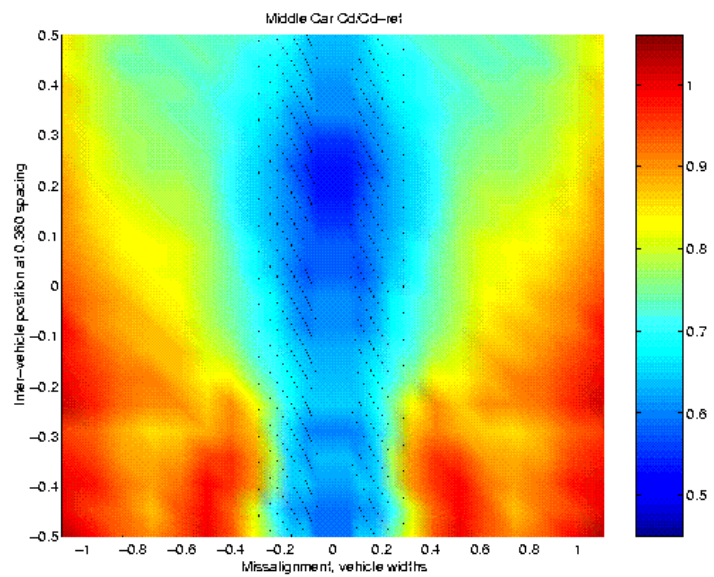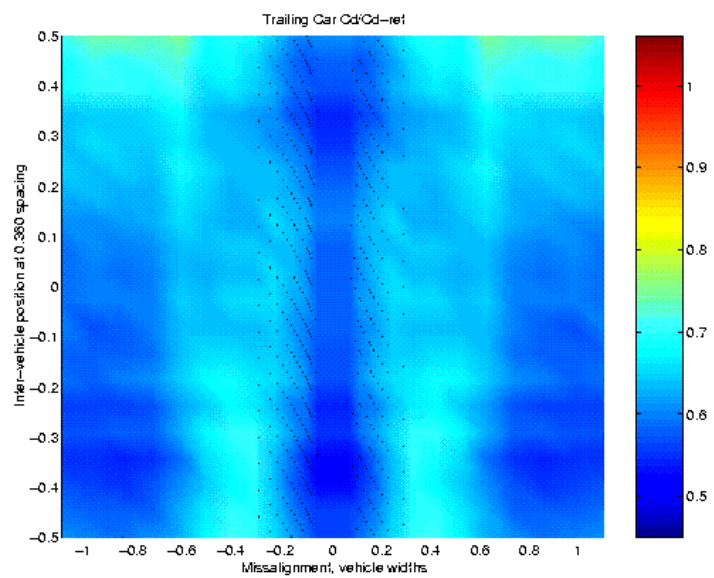
b) Middle Car

Middle Car Cd/Cd-ref
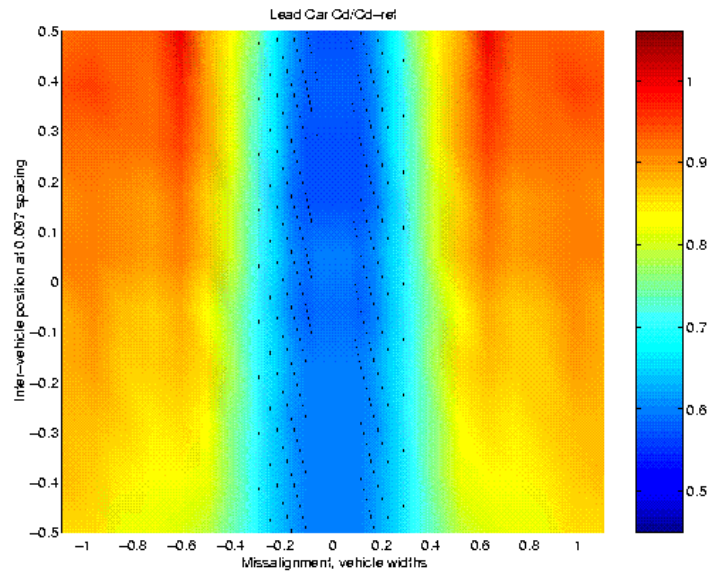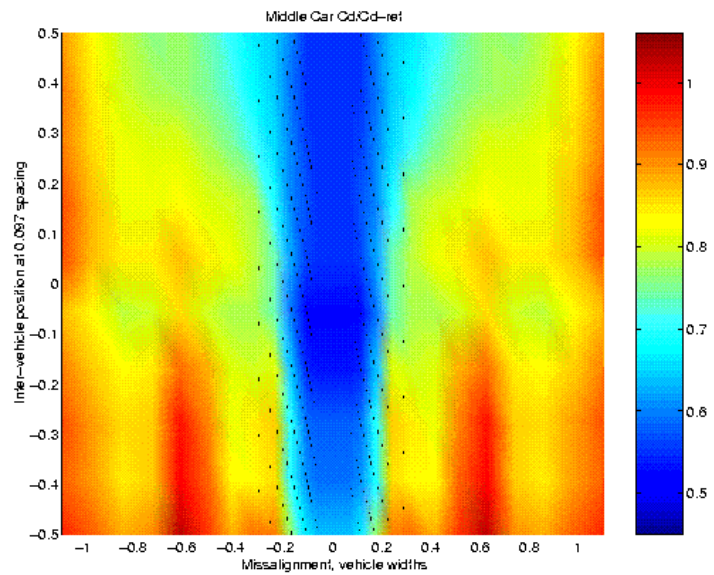
c) Trailing Car

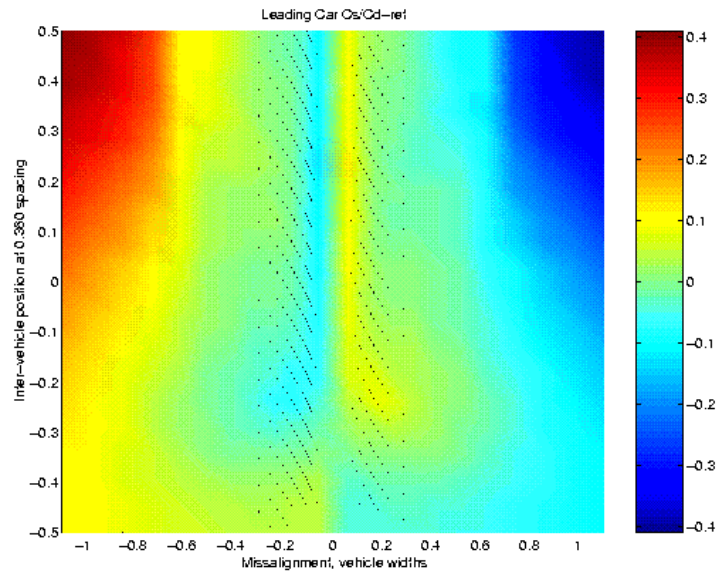**Figure 10**. Drag coefficient ratio color maps for non-symmetric vehicle positioning in the platoon. at 0.1 car lengths spacing

Trailing Car Cd/Cd-ref

a) Leading vehicle

Leading Car Cs/Cd-ref

b) Middle vehicle

Middle Car Cs/Cd-ref

c) Trailing vehicle

Figure 11. Side force coefficient ratio color maps for non-symmetric vehicle positioning in the platoon. at 0.1 vehicle lengths spacing

Trailing car Cs/Cd-ref

a) Leading vehicle

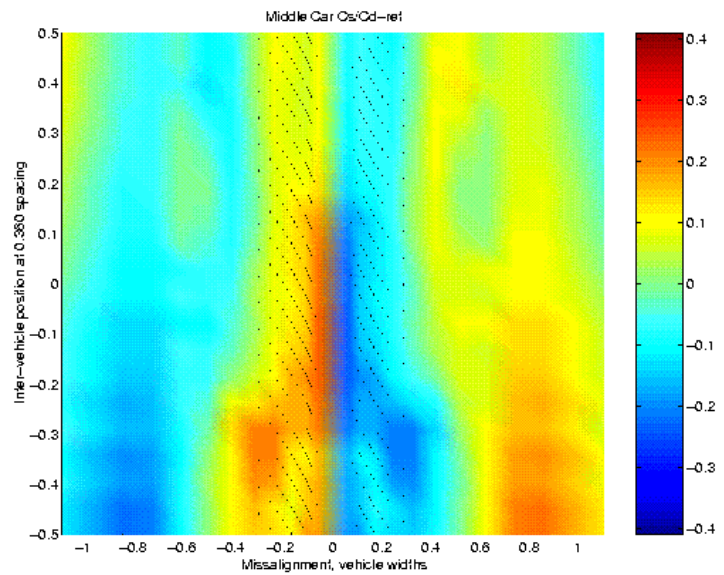**b)** Middle vehicle

c) Trailing vehicle

Figure 12. Yawing moment coefficient ratio color maps for non-symmetric vehicle positioning in the platoon. at 0.1 vehicle lengths spacing

a) Leading vehicle

b) Middle vehicle
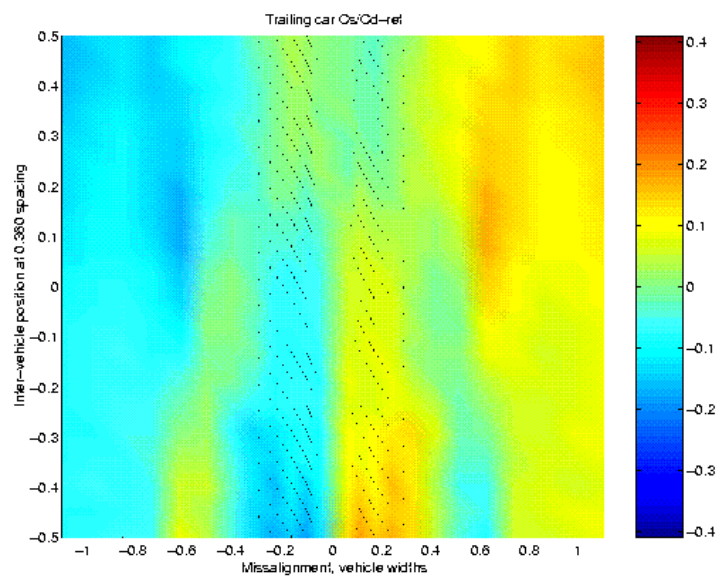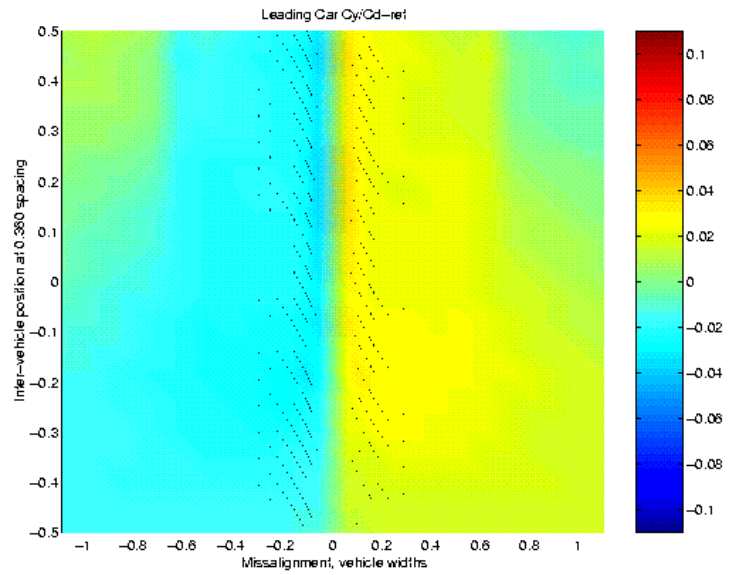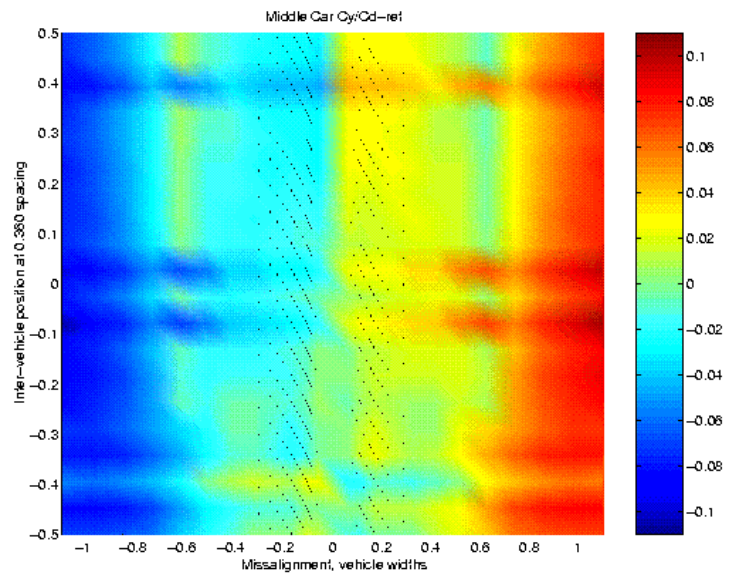
c) Trailing vehicle

Figure 13. Drag coefficient ratio color maps for non-symmetric vehicle positioning in the platoon. at 0.21 vehicle lengths spacing

a) Leading vehicle

Leading Car Cs/Cd-ref

b) Middle vehicle

Middle Car Cs/Cd-ref

c) Trailing vehicle

Figure 14. Side force coefficient ratio color maps for non-symmetric vehicle positioning in the platoon. at 0.21 vehicle lengths spacing

Trailing car Cs/Cd-ref

a) Leading vehicle

b) Middle vehicle
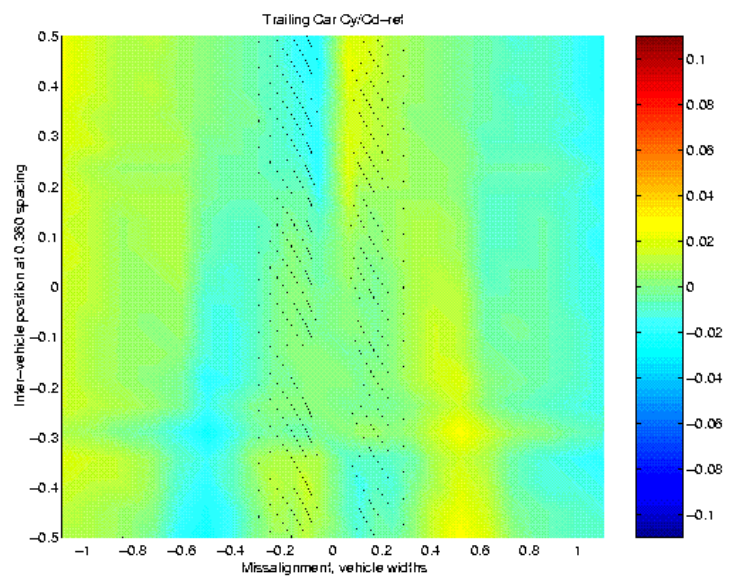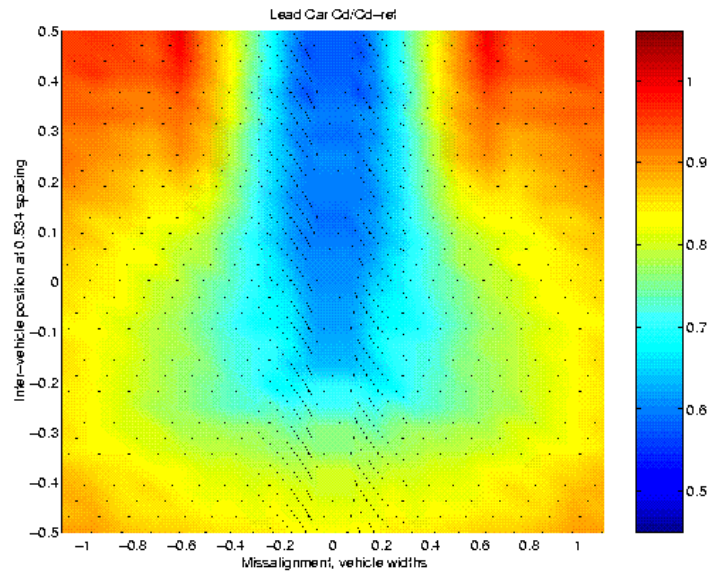
c) Trailing vehicle

Figure 15. Yawing moment coefficient ratio color maps for non-symmetric vehicle positioning in the platoon. at 0.21 vehicle lengths spacing

a) Leading vehicle

Lead Car Cd/Cd−ref

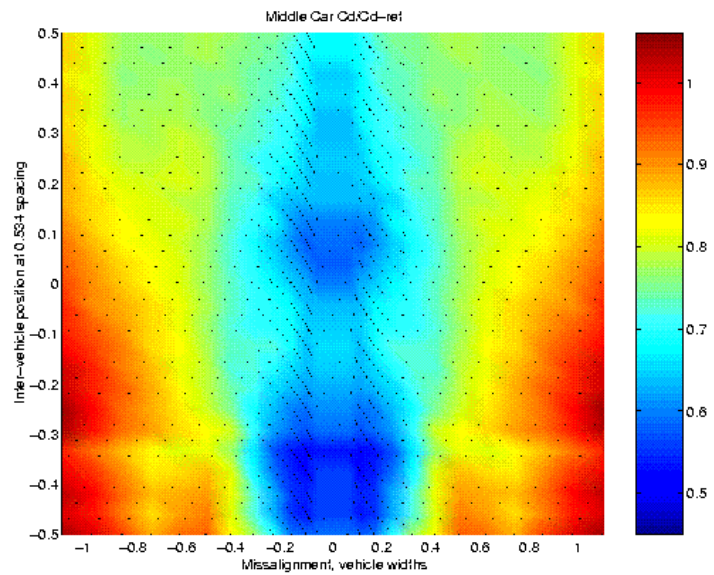**b)** Middle vehicle

Middle Car Cd/Cd−ref

c) Trailing vehicle

Figure 16. Drag coefficient ratio color maps for non-symmetric vehicle positioning in the platoon. at 0.36 vehicle lengths spacing

Trailing Car Cd/Cd−ref

a) Leading vehicle

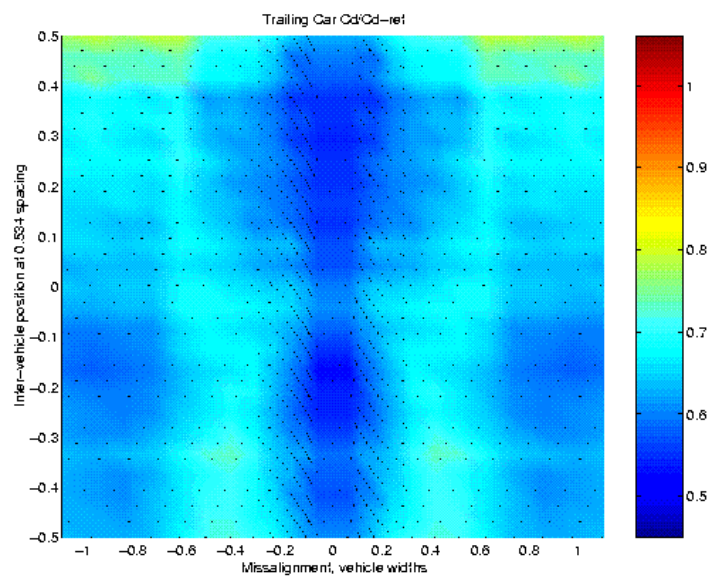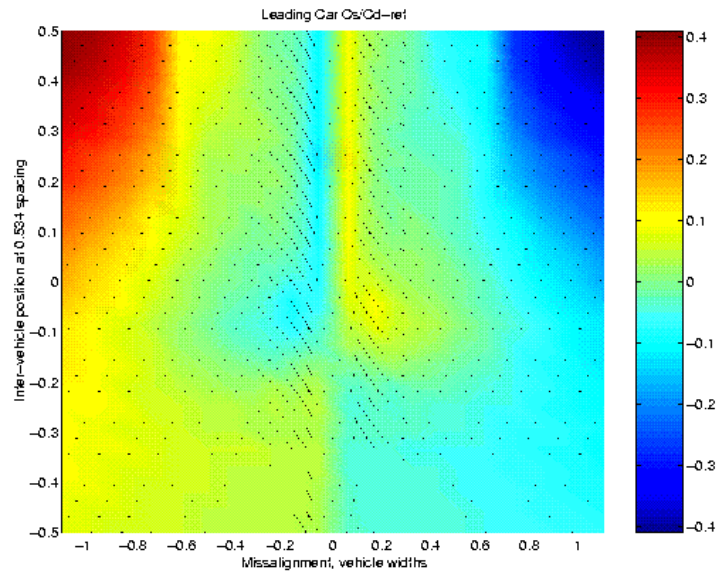**b)** Middle vehicle

c) Trailing vehicle

Figure 17. Side force coefficient ratio color maps for non-symmetric vehicle positioning in the platoon. at 0.36 vehicle lengths spacing

a) Leading vehicle

Leading Car Cy/Cd−ref

b) Middle vehicle

Middle Car Cy/Cd−ref

c) Trailing vehicle

Figure 18. Yawing moment coefficient ratio color maps for non-symmetric vehicle positioning in the platoon. at 0.36 vehicle lengths spacing

Trailing Car Cy/Cd−ref

a) Leading vehicle

Lead Car Cd/Cd−ref

b) Middle vehicle

Middle Car Cd/Cd−ref

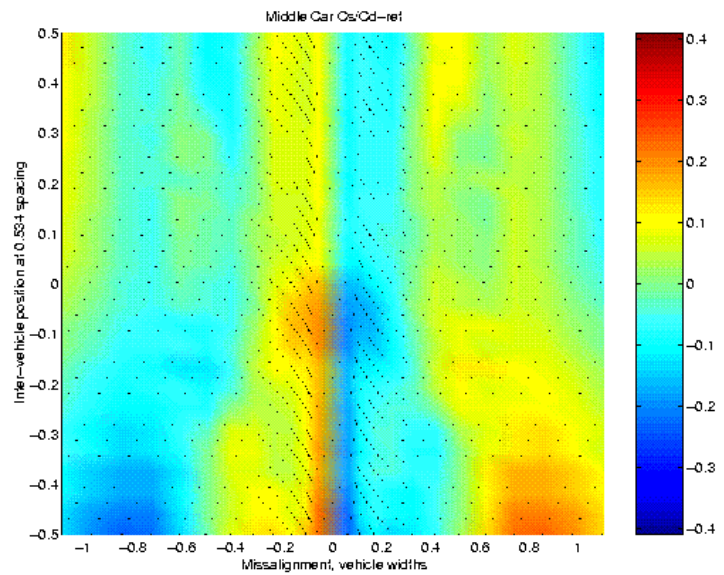**c)** Trailing vehicle

Trailing Car Cd/Cd−ref

Figure 19. Drag coefficient ratio color maps for non-symmetric vehicle positioning in the platoon. at 0.53 vehicle lengths spacing

a) Leading vehicle

b) Middle vehicle
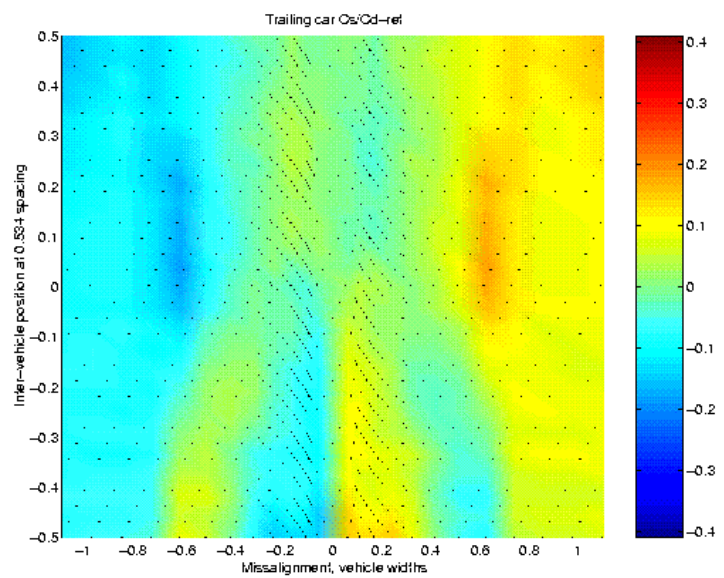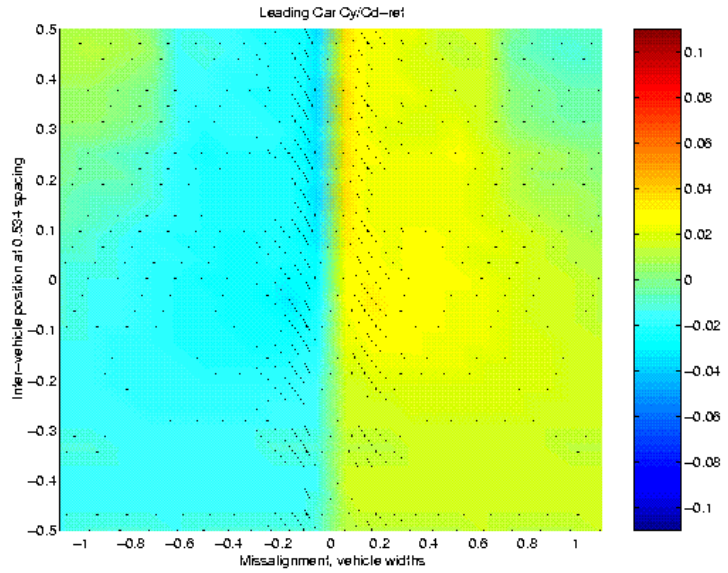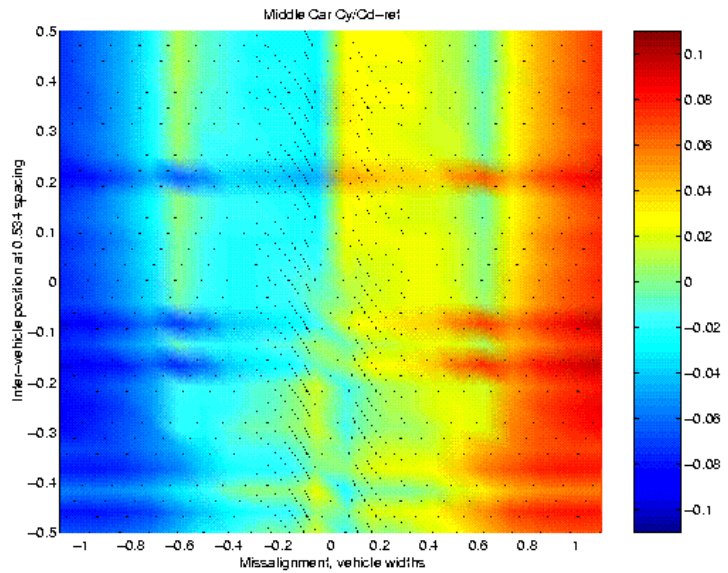

c) Trailing vehicle

Figure 20. Side force coefficient ratio color maps for non-symmetric vehicle positioning in the platoon. at 0.53 vehicle lengths spacing

a) Leading vehicle

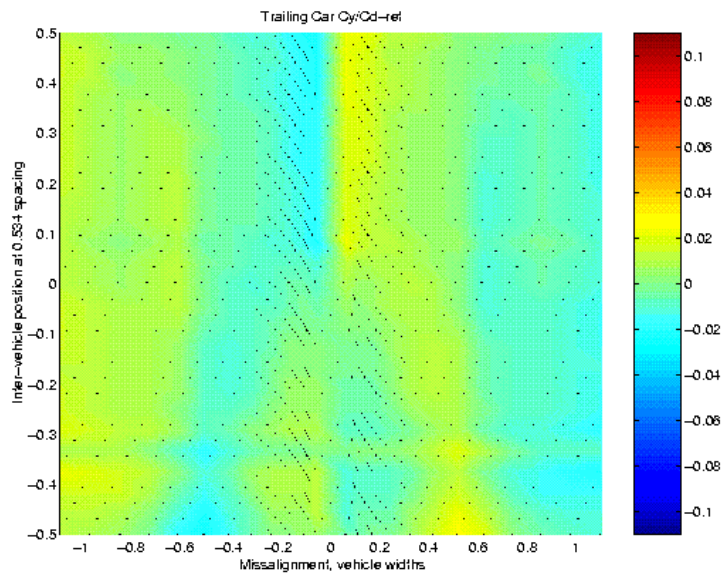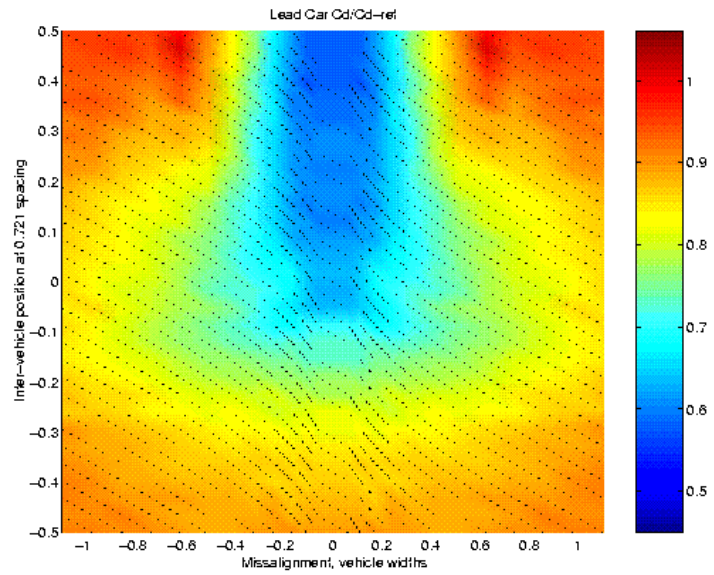**b)** Middle vehicle

c) Trailing vehicle

Figure 21. Yawing moment coefficient ratio color maps for non-symmetric vehicle positioning in the platoon. at 0.53 vehicle lengths spacing

a) Leading vehicle

b) Middle vehicle

c) Trailing vehicle

Figure 22. Drag coefficient ratio color maps for non-symmetric vehicle positioning in the platoon. at 0.72 vehicle lengths spacing

a) Leading vehicle

b) Middle vehicle

c) Trailing vehicle

Figure 23. Side force coefficient ratio color maps for non-symmetric vehicle positioning in the platoon. at 0.72 vehicle lengths spacing

a) Leading vehicle

Leading Car Cy/Cd-ref

b) Middle vehicle

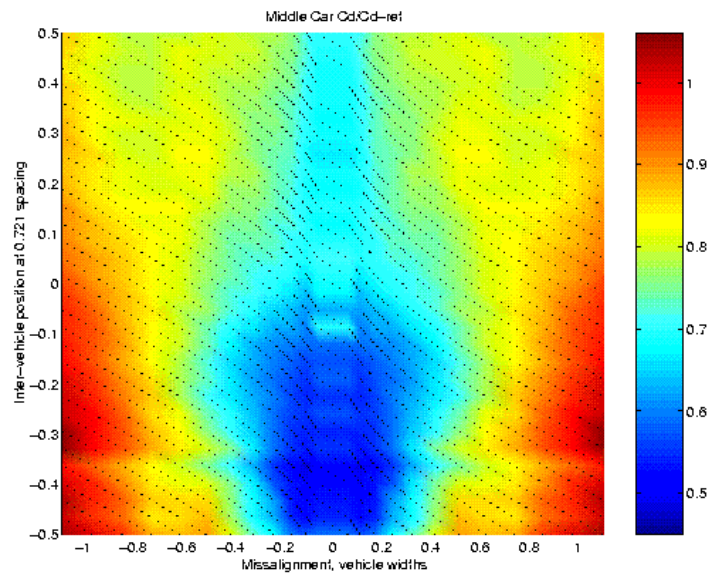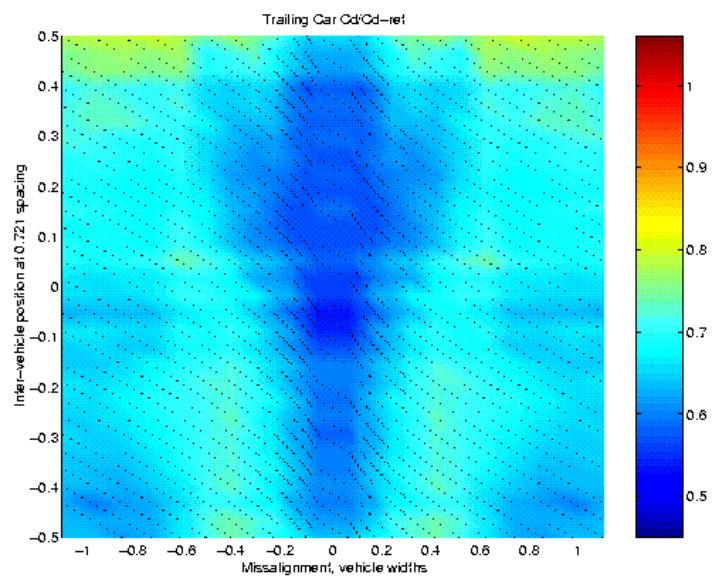Middle Car Cy/Cd-ref

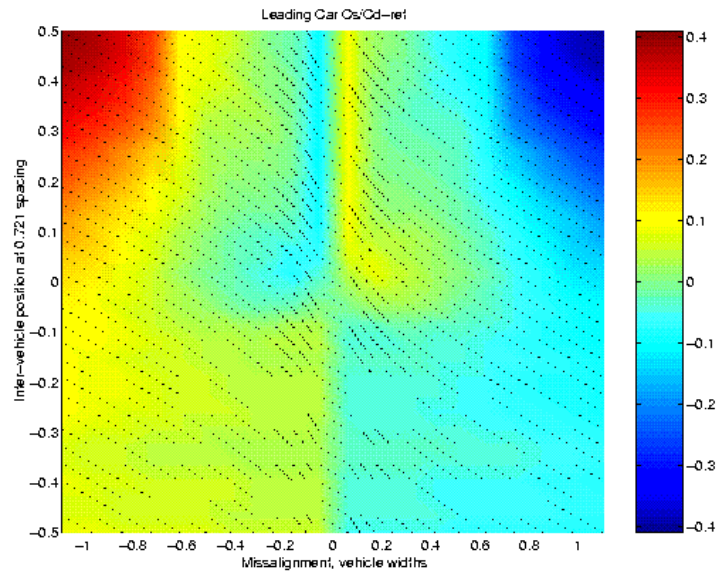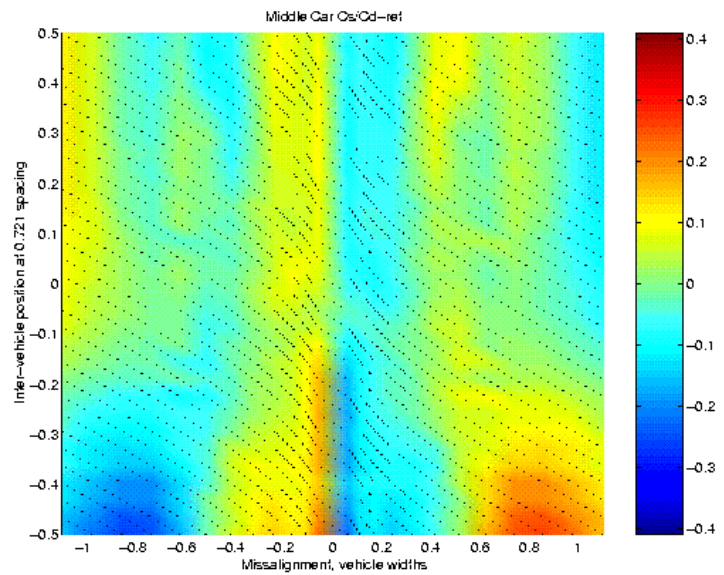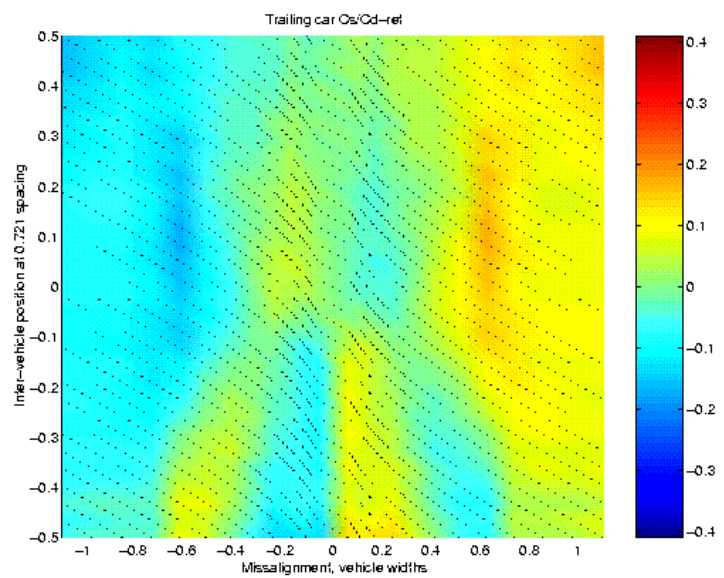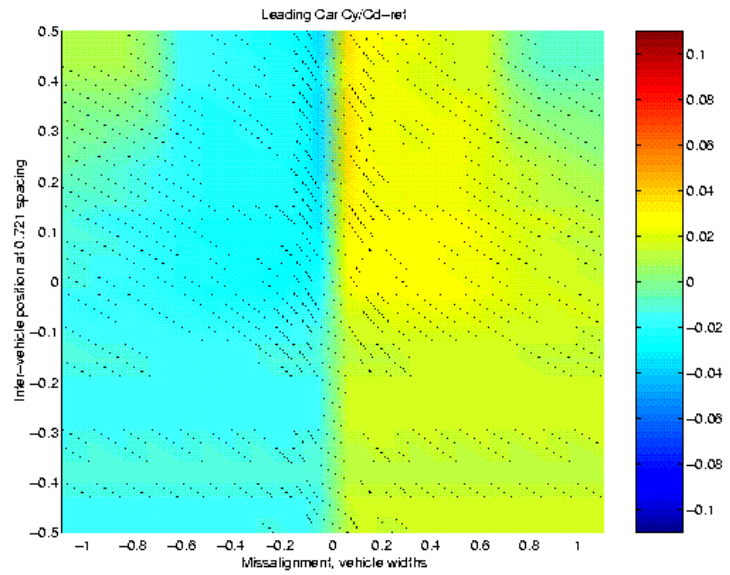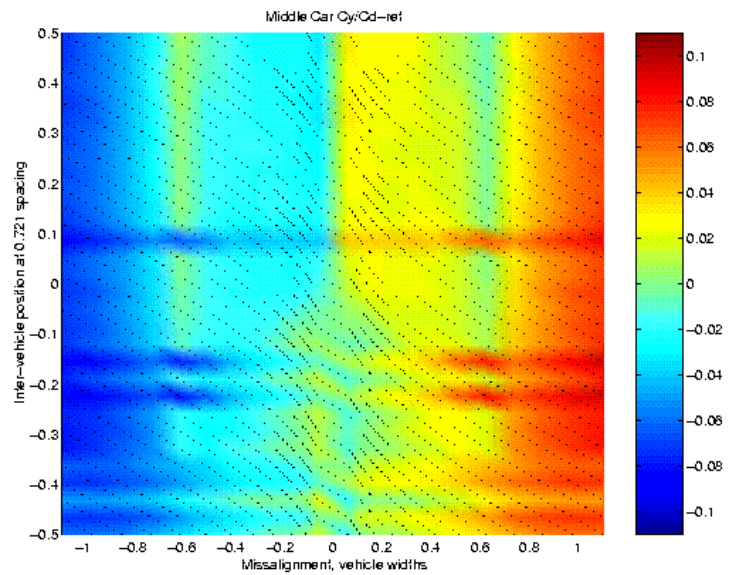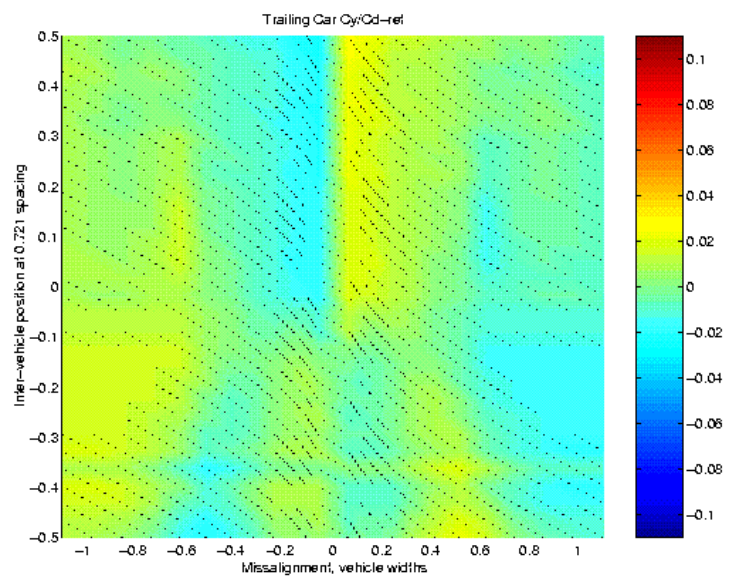**c)** Trailing vehicle

Figure 24. Yawing moment coefficient ratio color maps for non-symmetric vehicle positioning in the platoon. at 0.72 vehicle lengths spacing

Trailing Car Cy/Cd-ref

33

For longitudinal spacing of 0.72 vehicle lengths drag, side force and yawing moment coefficient ratio maps are shown in figures 22 through 24. At this spacing, non-symmetry effects are stronger on the drag experienced by the leading the middle vehicles. Smaller effects are observed on the trailing vehicle. For the first time, a "wave"-like structure is observed at longitudinal displacement of -0.35 for the middle vehicle. We believe that such variation in drag may be the result of a resonant type of flow, similar to the one described in Section IV of this report. Weaker variation of the same nature can be observed on the trailing vehicle. Interestingly, the "wave" structure observed on the yawing moment coefficient maps for the middle vehicle do not coincide in the longitudinal displacement values with the structure observed on the drag coefficient ratio map for the same vehicle.

4. Platoon averaged results

The average of the drag coefficient ratios for the entire platoon provide a measure of misaligned platoon performanc (side forces and yawing moment are quantities of individual nature for each vehicle). The average drag coefficient ratio is calculated as

$$(C_{Dp})_{avg}/C_{D\infty} = \left(\frac{1}{n}\right) \sum_{i=1}^{n} (C_{Di}/C_{D\infty})$$

For all of the symmetric configurations investigated, a drag coefficient ratio map is shown in figure 25. At very short longitudinal spacings (less than 0.05 vehicle lengths) interactions of stronger nature increase the drag when misalignment is larger than 0.3 vehicle widths. For longitudinal spacing larger than 0.2 vehicle lengths the platoon sensitivity to misalignment (drag-wise) increases with the longitudinal vehicle spacing.
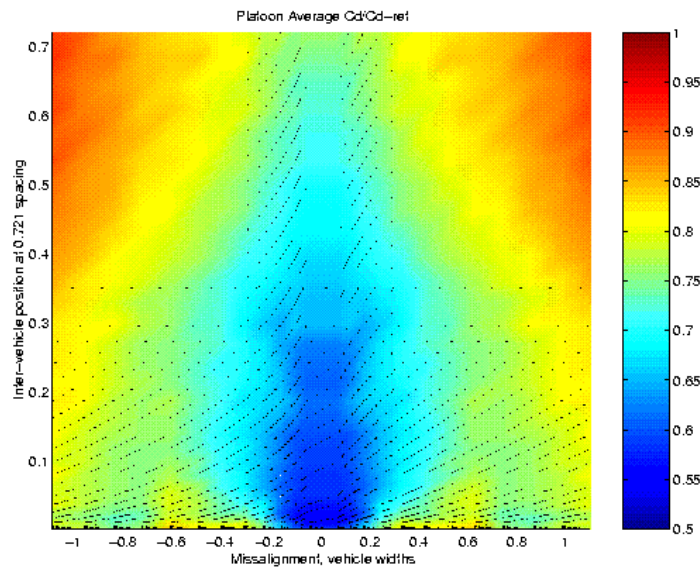
Figure 25. Platoon averaged drag coefficient ratio colormap for symmetric vehicle spacing.

34

Figure 26 shows platoon averaged drag coefficient ratio maps for non-symmetric configurations corresponding to a) 0.1 vehicle lengths spacing, b) 0.21 vehicle lengths spacing, c) 0.36 vehicle lengths spacing, d) 0.53 vehicle lengths spacing, and e) 0.72 vehicle lengths spacing. At short spacings such as 0.1 and 0.21 vehicle lengths, non-symmetry effects are small for the platoon averaged drag performance. For 0.53 vehicle lengths separation, the lowest drag values, at small misalignments, is observed for closer spacing between leading and middle vehicles, over a range of longitudinal displacements of 0.1 to 0.4. The lowest sensitivity to large misalignments is observed around zero longitudinal displacement, i.e. around the symmetric configuration. Similarly, for 0.72 vehicle lengths separation, the lowest sensitivity to large misalignments is also observed around the symmetric configuration.

a) Non-symmetric, 0.1L
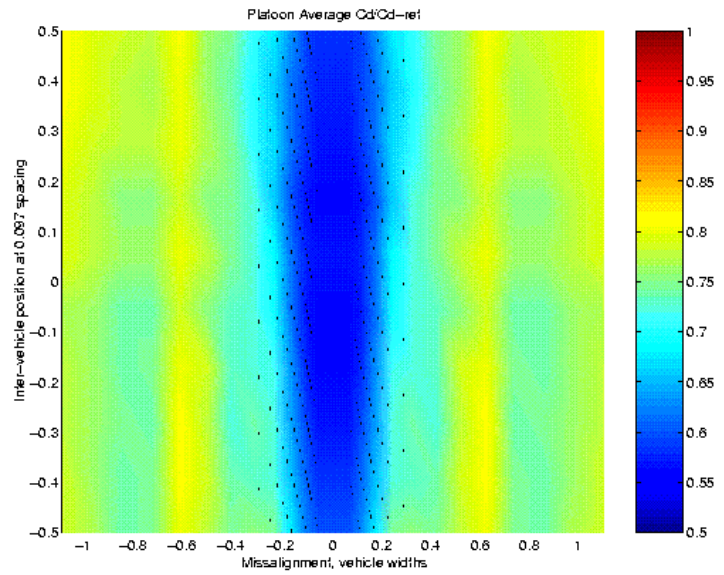
b) Non-symmetric, 0.21L
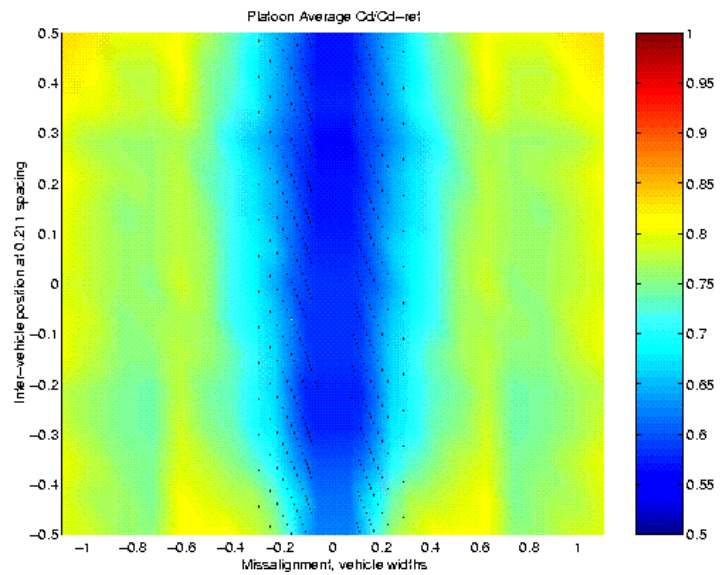
c) Non-symmetric, 0.36L

Figure 26. Platoon averaged drag coefficient ratio color maps for non-symmetric vehicle spacing in the platoon.

d) Non-symmetric, 0.53L

e) Non-symmetric, 0.72L

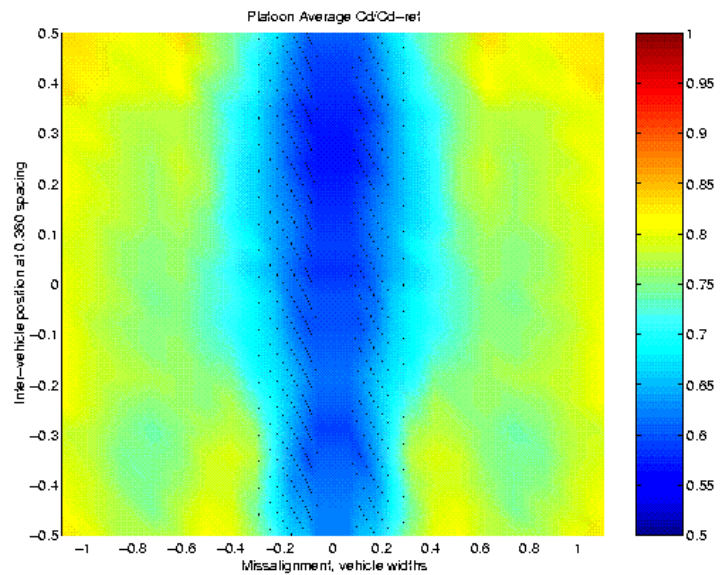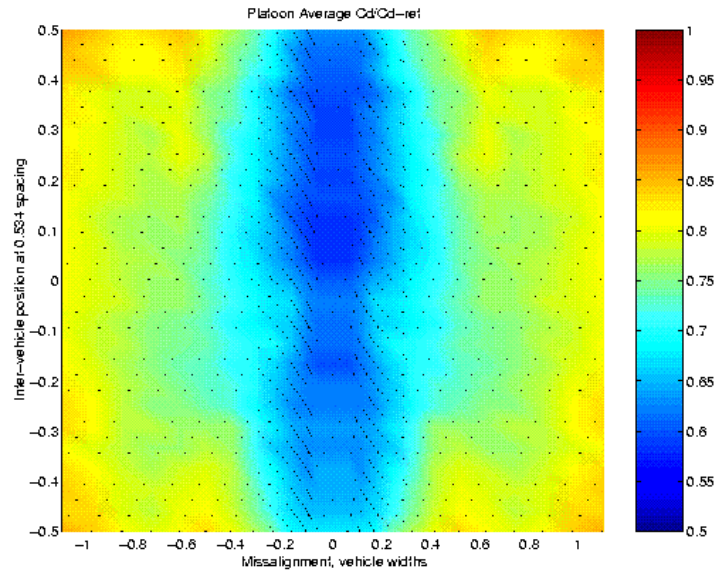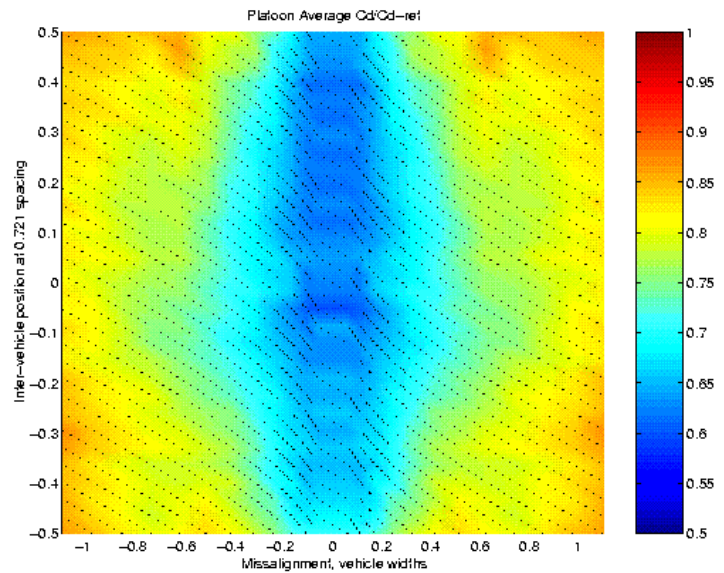**Figure 26 (continued)**. Platoon averaged drag coefficient ratio color maps for non-symmetric vehicle spacing in the platoon.

IV. Quasi-Steady Forces on Two Misaligned Vehicles: Back-to-Back Geometry

1. Large gradient in drag force observed at small spacings

The *back-to-back* geometry refers to the case in which the lead vehicle is in a normal attitude, but the orientation of the trail vehicle is reversed. Since the backs of the vans are almost flat, the back-to-back geometry provides a nearly uniform gap (spacing) between the vehicles, as in figure 27. It was discovered in our previous work (Zabat et al. 1995), that as vehicle spacing decreases towards 0.1 vehicle lengths, the drag first decreases, then almost doubles in magnitude to a local maximum before decreasing again. This rapid rise and decrease was shown to take place as the vehicle separation changes by less than 0.1 vehicle lengths, although at the time there was insufficient spatial resolution to properly define the details of the peak. We now return to study this interesting case utilizing stepper-motor-controlled positioning for both vehicles, which allows much finer spatial resolution to be achieved.
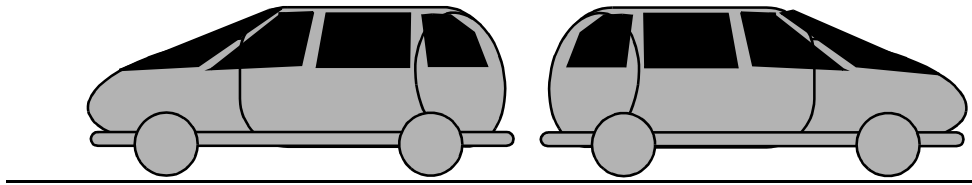

Figure 27. Back to Back geometry

Back-to-back geometry is an example of a geometry which is quite distinct from the normal, forward facing arrangement. We should not be surprised if this case presents certain differences from the normal arrangement, because it is clear from previous results that vehicle geometry will be an important parameter at short spacings. Although a back-to-back arrangement is more extreme than is likely to be encountered with automobile vehicles, similar drag peaks do arise for more conventional geometries for similar reasons we believe. Back-to back geometry is relevant to close-following trucks, which are generally much blunter in shape. The results are also relevant to the *gaps* between tractors and trailers and between trailers (for large multi-trailer rigs).   For all these reasons we feel it is important to document and understand the back-to-back results.

2. Special set-up and procedure

The experiment is assembled in the Dryden Wind Tunnel utilizing two of the minivan models placed back-to-back along the centerline of the tunnel. Although the drag rise–we refer to it as a resonance peak for reasons to be described later–was previously observed using either porous or solid ground plane (Zabat et al. 1995), the floor of the wind tunnel is now covered with adhesive shelf paper in the vicinity of the models to eliminate any possibility that the effect is somehow related to suction through the porous groundplane.

In re-examining the resonance we feel it is also important to allow the vehicles to be displaced

laterally. The lateral misalignment is small, no more than about 2.5 per cent of the vehicle width (0.025 W, where W = 23.46 cm). The total misalignment is divided into twelve steps, each step representing a lateral motion of 0.00198 W. The longitudinal separation travel is chosen to be 0.72 vehicle lengths (L = 61.6 cm). This travel is divided into 49 steps of 0.0147 L spacing. The test matrix is 12 x 49 = 588 data points. Drag, side force and yawing moment are recorded for each vehicle for each position. These values are defined by eight second averages over 8192 data points (digitization rate of 1024 points per second per channel). Two separate tests are conducted, one test utilizes a rubber band trip placed around the lead vehicle approximately 1/3 of the way along the surface, and one test is performed without artificial tripping. The former experiment is referred to as the tripped experiment. No significant differences are observed in forces and moments as a result of tripping, but small variations do occur between the two experiments.

As will become evident, it is also necessary to describe the sequence of movements of the two vehicles. The experiment commences with the trailing vehicle at its extreme position, -.015W, and the vehicle bumpers touching (zero longitudinal spacing). The position of the leading vehicle is incremented forward until it reaches the extreme spacing, +.721L. The lateral position of the trailing vehicle is incremented, and the leading vehicle returns by steps to zero longitudinal spacing. This sequence is repeated (six times) until the lateral position of the trailing vehicle reaches the positive extreme position, +.01W.

3. Results

The results are contained in figures 28-31. Figure 28 presents drag, side force and yawing moment for the leading vehicle, and figure 29 gives identical information for the trailing vehicle. Figures 30 and 31 present similar information for the tripped runs. Coefficient values of drag, side force and yawing moment are presented as level color surfaces in a two-dimensional plot. The two space coordinates represent (longitudinal) spacing between vehicles (in fractions of vehicle length), and lateral misalignment (in fractions of vehicle width). The total lateral misalignment is a very small distance in comparison to the range of vehicle separations. Thus the geometry of the picture is highly distorted. Please also note that the color bars are different from those used previously for the three misaligned vehicles. Each plot is scaled with its own color bar, so the level curve values corresponding to a given color differ from plot to plot. Values are given alongside each color bar.

As discussed previously, the values presented here are ratios of drag coefficient, side force coefficient and yawing moment coefficient *normalized by the drag coefficient of the isolated vehicle measured at the identical position in the wind tunnel.* In this report, we refer to drag coefficient in isolation as C_{Dref}, or $C_{D\infty}$. For the trailing vehicle, the isolation drag coefficient is the drag coefficient for the vehicle in that same reversed orientation. These normalizing values are: for the trailing vehicle, reversed orientation,

C_{Dref} = 0.3146, measured at x = 252 cm from the ground plane origin (figure 2),

and for the leading vehicle,

C_{Dref} = 0.281 ±0.004, measured between x = 148 cm and x = 192 cm.

a) Drag coefficient ratio
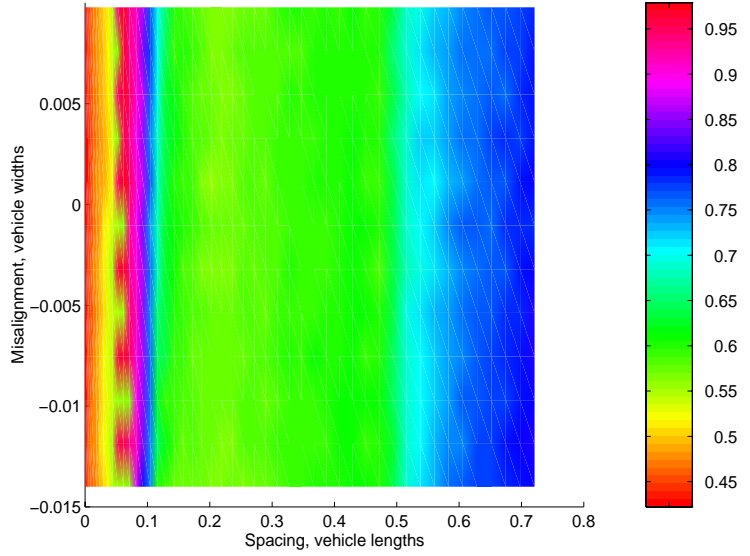
b) Side force coefficient ratio
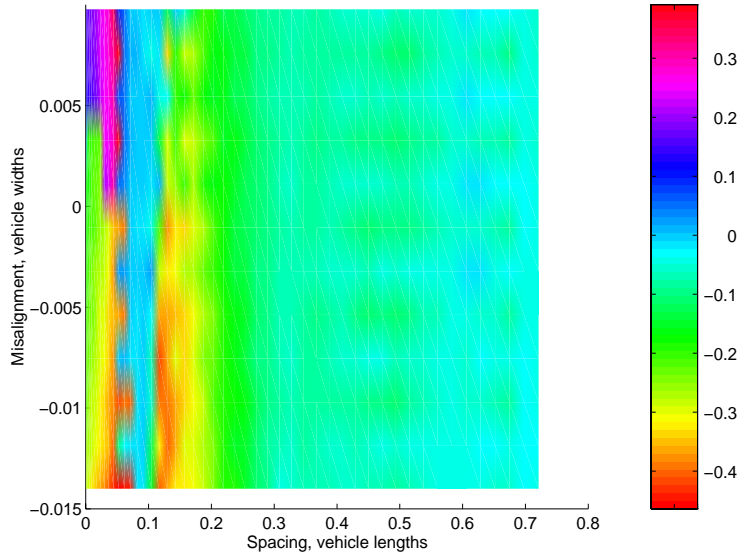
c) Yawing moment coefficient ratio

Figure 28. Force and moment coefficient ratio color maps for the leading vehicle in a back to back two-vehicle platoon configuration

a) Drag coefficient ratio

b) Side force coefficient ratio

c) Yawing moment coefficient ratio
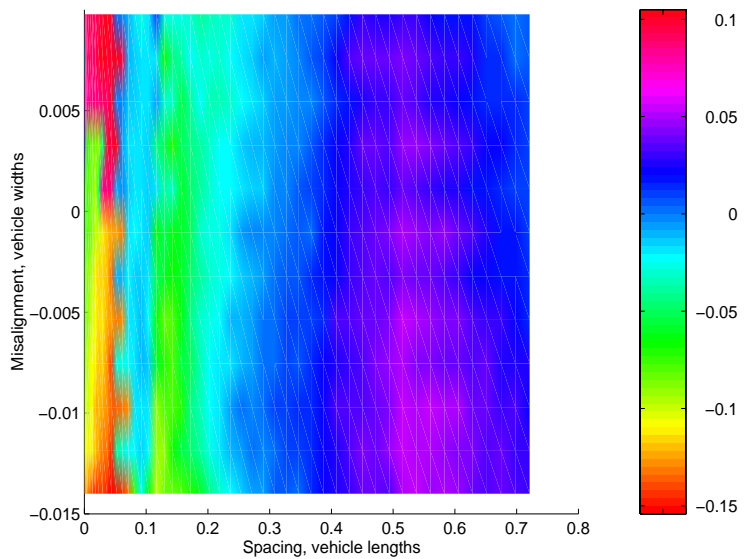
Figure 29. Force and moment coefficient ratio color maps for the trailing vehicle in a back to back two-vehicle platoon configuration

41

a) Drag coefficient ratio
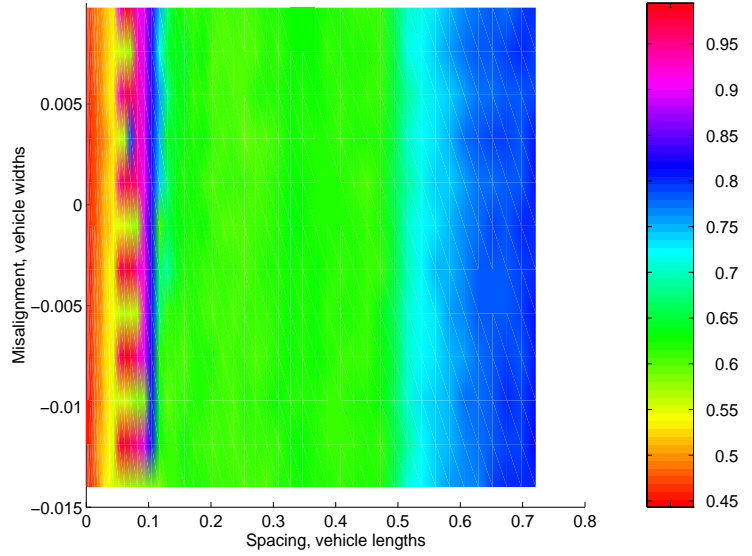
b) Side force coefficient ratio
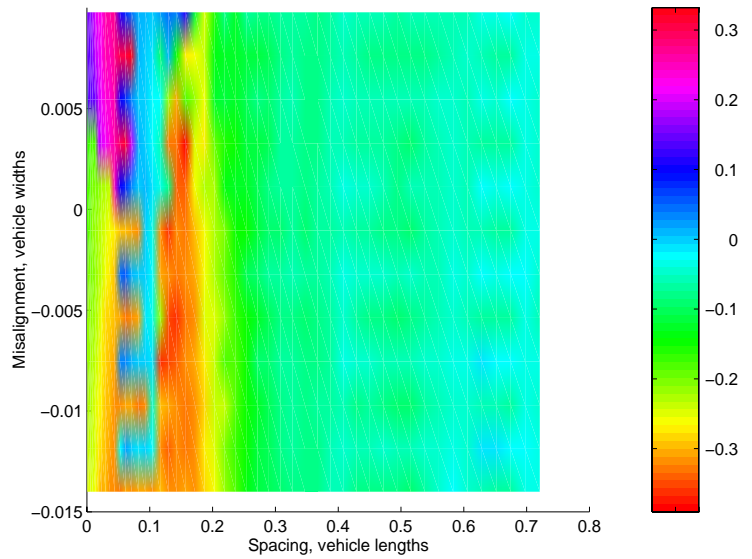
c) Yawing moment coefficient ratio
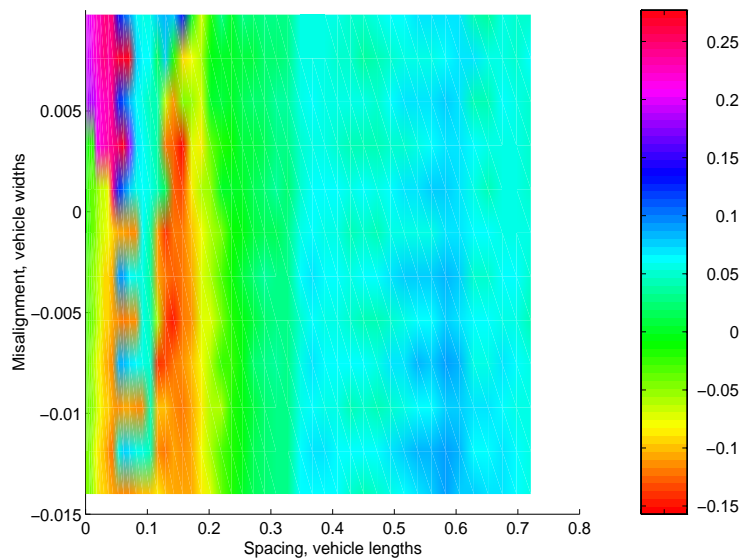
Figure 30. Force and moment coefficient ratio color maps for the leading vehicle in a back to back two-vehicle platoon configuration. Boundary layer is tripped on the leading vehicle.

42

a) Drag coefficient ratio
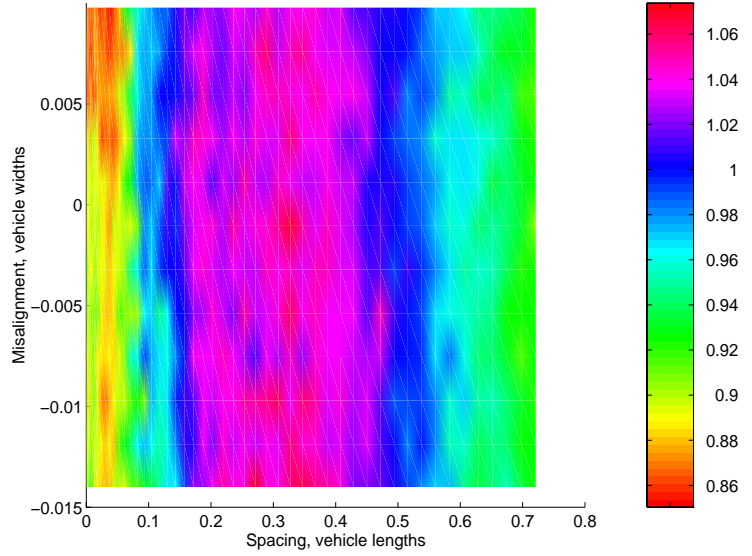
b) Side force coefficient ratio
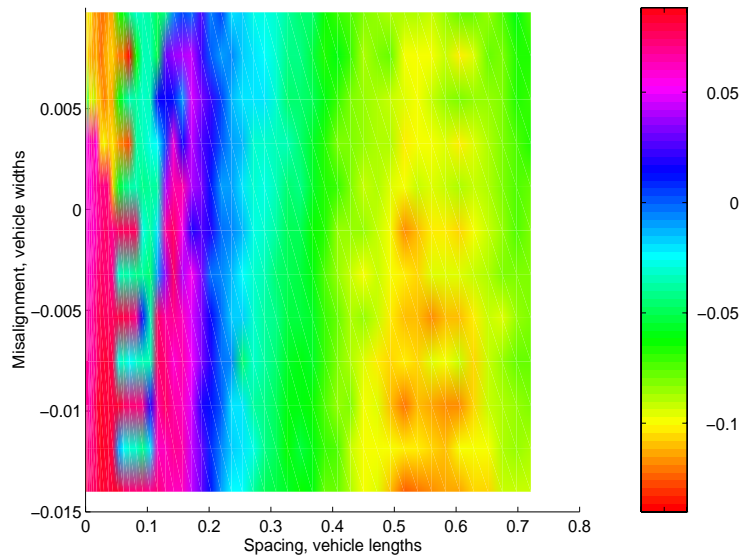
c) Yawing moment coefficient ratio

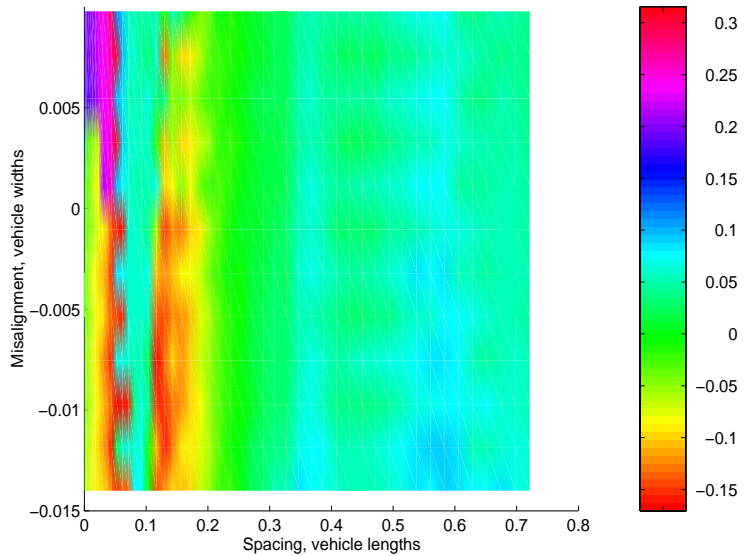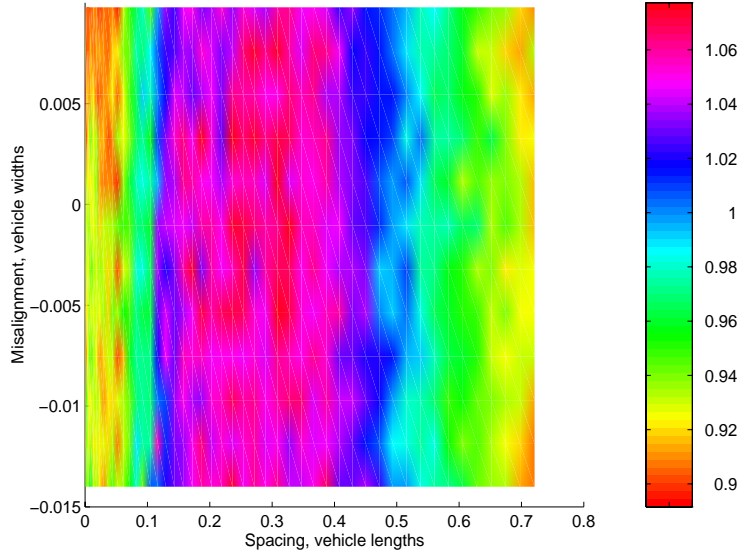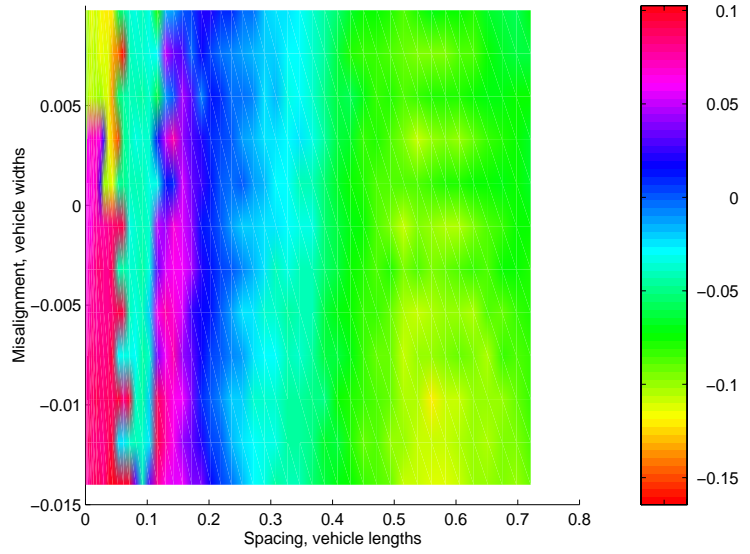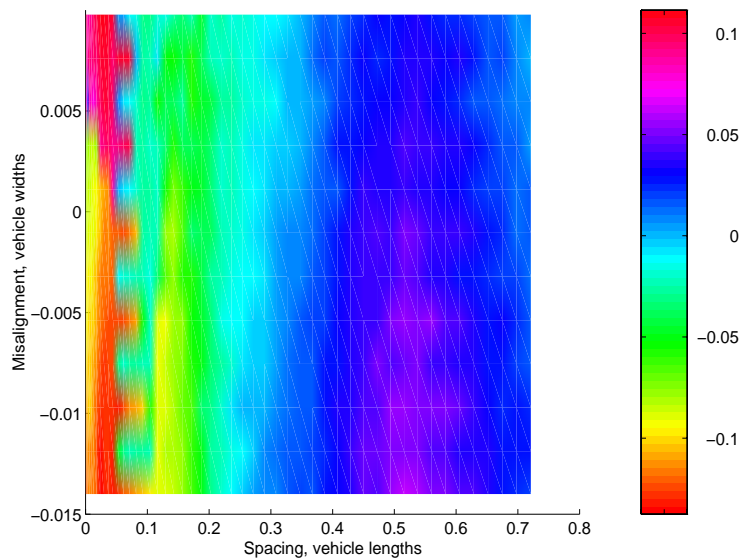**Figure 31.** Force and moment coefficient ratio color maps for the trailing vehicle in a back to back two-vehicle platoon configuration. Boundary layer is tripped on the leading vehicle
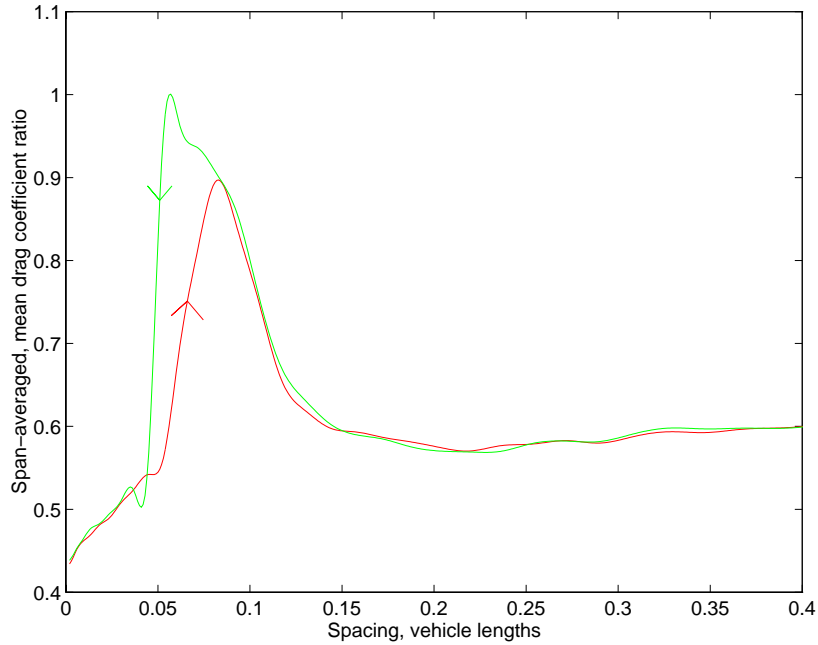
Figure 32. Span averaged drag coefficient ratio for the leading vehicle, without tripping. The averaging is done separately for the leading vehicle leaving the influence of the trailing vehicle and for the leading vehicle entering the influence of the trailing vehicle.
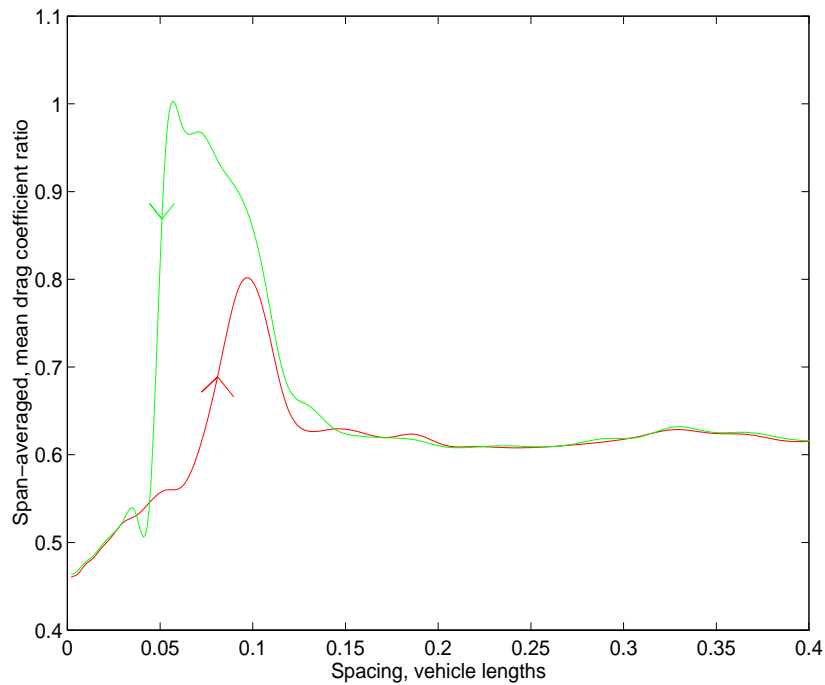
Figure 33. Span averaged drag coefficient ratio for the leading vehicle with boundary layer tripping. Averaging procedure similar to figure 32.
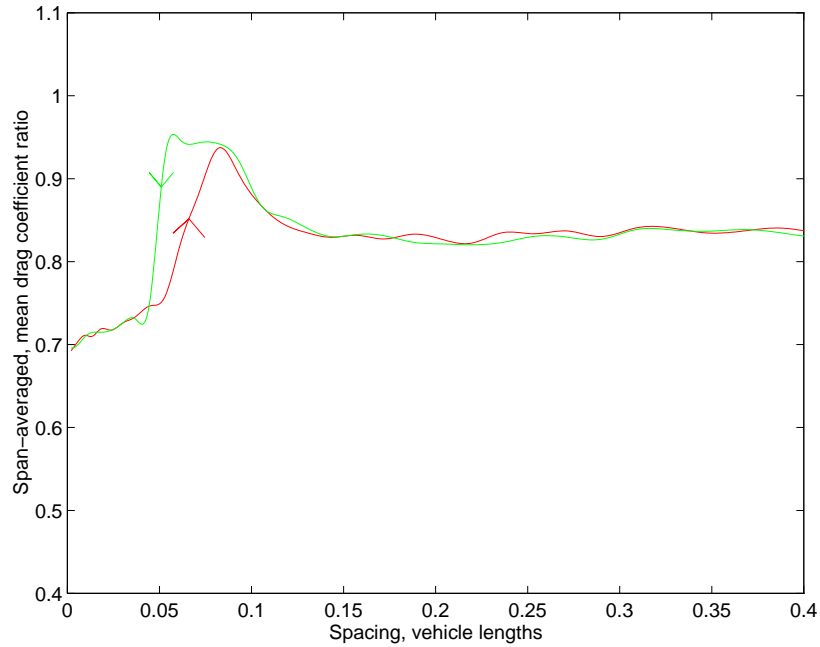
Figure 34. Drag coefficient ratio values averaged for both vehicles in back to back geometry without tripping of the boundary layer. Values are also span-averaged, separately for each travel as in figure 32
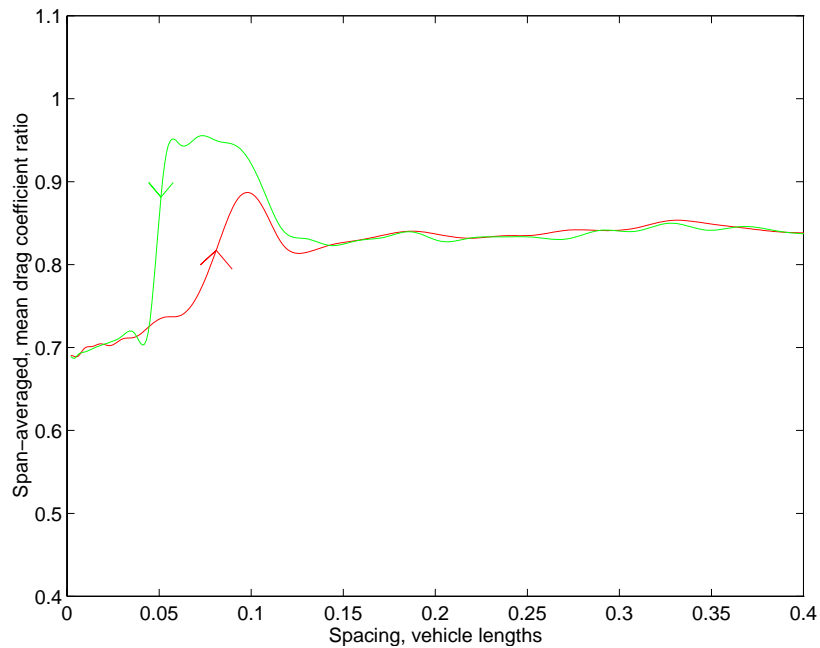
Figure 35. Drag coefficient values averaged of both vehicles in back to back geometry, with tripping of boundary layer on the leading vehicle. Values are span averaged as in figure 34.

Yawing moment is referenced to the center of the force balance, which lies on the vehicle centerplane at a distance of 0.4654 L measured from the rear bumper.

The most striking feature of the aerodynamic interaction between these two vehicles is the behavior of the drag (or drag coefficient) of the leading vehicle at short spacings, as shown in figure 28 a). Drag coefficient ranges from a low value of about 0.45 at zero spacing, rises to a peak value of $C_D/C_{Dref} = 0.95$-1.0 at a spacing of approximately 0.08L, before decreasing just as dramatically to value below $C_D/C_{Dref} = 0.58$-0.60 at a distance of 0.13L. This behavior takes place across all lateral positions of the trailing vehicle, although there is a fine structure which indicates a hysteresis, depending upon whether the leading vehicle is approaching or leaving the vicinity of the trail vehicle. The hysteresis shows itself as the 'toothed' shape of the color contours centered at about 0.082L. There are six reddish 'teeth' and six 'spaces' across the span. The 'spaces' correspond to forward travel of the lead vehicle as it gradually leaves the influence of the trail vehicle, and the 'teeth' correspond to the lead vehicle gradually entering the local flow field from a more forward position. The hysteresis loop can be established by averaging separately across the six 'spaces' and across the six 'teeth'. The result of such an average is shown in figure 32, where the direction of travel of the forward vehicle is also marked. An interpolating cubic spline has been fit to the trajectories. The identical procedure applied to the vehicle with boundary layer trip displays the slightly larger hysteresis loop shown in figure 33.

Interestingly, the second vehicle participates only minimally in the drag change as shown by the contours in figures 29 a) and 31 a). A mean drag coefficient can be defined as one-half the sum of the drag coefficients for each vehicle. Mean drag can also be ratioed with the mean drag of the two vehicles in isolation. Figures 34 and 35 present these *ratioed* results respectively for the vehicles without and with boundary layer tripping.

Both side force and yawing moment on the two vehicles change anti-symmetrically as the trail vehicle moves laterally across the centerplane. The total changes in side force and yawing moment (with movement across the centerplane) are a significant fraction of the drag force in isolation, but any significant effect is confined to very short spacings–of the order of 0 - 0.2 vehicle lengths. Force and yawing moment changes are larger for the leading vehicle than for the trail vehicle by about a factor of two. Recall however, that the normalizing value of drag coefficient in isolation is higher for the second vehicle, so the actual magnitudes of the forces on the two vehicles will differ by less than a factor of two. Tripping the boundary layer on the lead vehicle reduces side force and yawing moment values slightly.

4. Discussion

Tripped boundary layer versus non-tripped boundary layer. In wind tunnel tests utilizing models operating at Reynolds numbers less than those associated with full scale operation, it is sometimes useful to employ an artificial tripping device such as the stretched rubber band used here. Tripping the boundary layer insures that the flow becomes fully turbulent at a specified location, and allows a greater confidence to extend the model results to higher values of Reynolds number. In our case, the observed differences in measured forces are small. The model Reynolds

number is sufficiently large to promote transition to turbulence naturally. We have confidence that the wind tunnel predictions are not terribly sensitive to changes in Reynolds number, and that the differences observed between the tripped and non-tripped results are probably suggestive of the differences one might expect in extending the Reynolds number to full scale values. There is one noticeable and persistent difference between the tripped and non-tripped data. Almost all of the plots (in figures 28 - 31) show the hysteresis to be slightly more pronounced when tripping is employed. The reason is not clear, but it may be associated with the establishment of a more nearly uniform boundary layer thickness around the perimeter of the leading vehicle at the point of flow separation from the top and sides.

Side force and yawing moment. The directions of the side forces and yawing moments lend themselves to a simple interpretation by reference to figure 36. The darkened arrows give the measured directions for side force and moment on each of the two vehicles (viewed from above) at the two extremes of misalignment. Note the sketches magnify the misalignments, which are actually much smaller. Also sketched are the outer flow streamlines, which must curve as indicated over the rearmost portion of the lead vehicle and the over the forward portion of the trail vehicle.
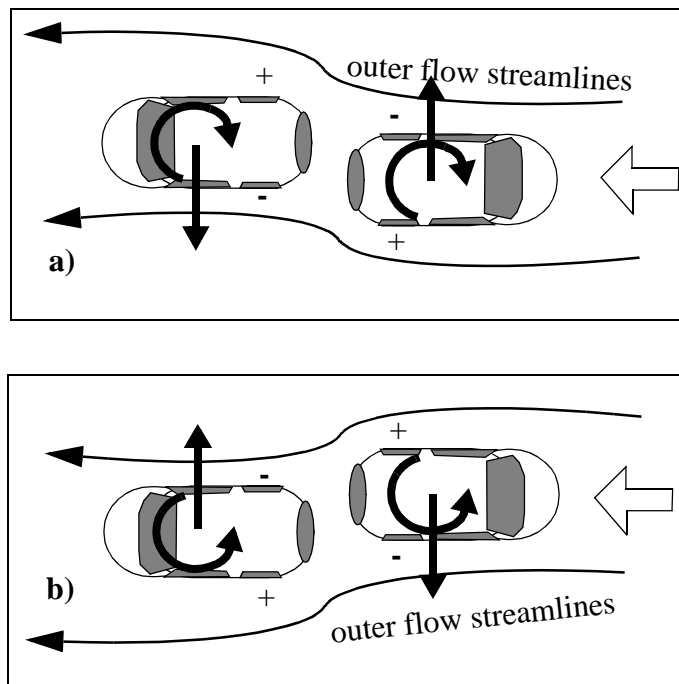
Figure 36. Generation of side forces and yawing moments by air flow patterns generated by misalignment geometry.

The curvature of the outer flow streamlines results in the pressure excesses and defects indicated by the small plus and minus values on the sides of the vehicles. The pluses and minuses are consistent with the directions of the resultant side forces and yawing moments. The side forces generated by misalignment are stabilizing in the sense that the side forces tend to reduce the misalignment. The yawing moments are stabilizing also, in the sense that they would again act to diminish the degree of misalignment.

Drag rise as a 'resonance' in the separating flow. One possible explanation for the large increase in drag at short vehicle spacing is that it represents a 'resonance' between the turbulence structure - structure within the shear layer forming the boundary of the separated region between the vehicles - and the spacing itself. Figure 37 is a sketch of the two vehicles with focus upon the spacing, or gap between them. It might also be helpful to think of the gap region as a cavity having three open sides. Let the thickness of the turbulent shear layer be given the symbol δ, the natural separation distance between large turbulent structures within the shear layer be given the symbol λ, and the length of the separated region, or cavity, be denoted by S_G. Then suppose the impingement of a turbulent structure at the downstream end of the cavity gives rise to a small pressure disturbance which travels upstream and excites the formation of another turbulent structure. (Since the gap is short and the speed of sound large, the time interval between impingement and excitation is negligibly short.) It is then easy to see that a gap length equal to an integer multiple of λ, say $n\lambda$, will correspond to a special circumstance, since each arriving structure will excite a new structure at the precise time most advantageous for the promotion of the natural turbulent structure. Such resonances commonly occur in fluid mechanic applications. (Closely related observations were discussed by Roshko & Koenig (1978), and by Gharib & Roshko (1987), as pointed out in an earlier version of the present argument (Browand, Zabat & Tokumaru (1997) The argument can be made more quantitative by noting that for a developing turbulent shear layer, $\lambda = 7\text{-}8\delta$, and that for our wind tunnel test, $Re_L \cong 10^6$, δ will be of the order of 1-1.2 centimeters. Referring to figure 33, the peak in the 'resonance' curve occurs at a spacing of 0.05L = 3.1 centimeters. Adding to this the average spacing remaining when the back bumpers touch, 7.4 centimeters, gives a total spacing of about 10.5 centimeters for resonance. Since 8 x 1.2 cm is approximately this same distance, we conclude that the resonance occurs in the lowest mode, that is for $S_G = \lambda$, and n = 1. The presence of the hysteresis loop currently remains unexplained.
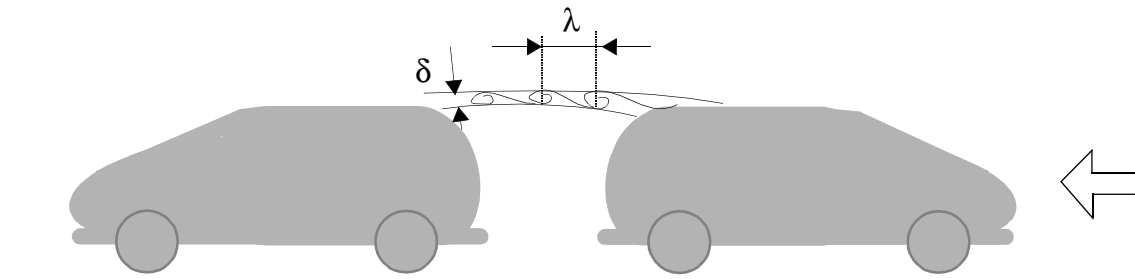
Figure 37

The resonance occurring in the case of *back-to-back* geometry is particularly strong, we believe, owing to the uniformity of the dimensions of the gap. However, many lesser peaks appear in the flow field of closely spaced vehicles. In section III, peaks are shown in the yawing moment coefficient ratios for most symmetric and non-symmetric three-vehicle platoon configurations over a wide range of misalignments. Another example is the four-vehicle platoon configuration reproduced in figure 38 the drag results from Zabat et al. (1995). Note the substantial peak in the drag of the third vehicle at a spacing of approximately 0.1L, and the two smaller peaks in the drag curve for the second vehicle (at about 0.1L and 0.3L). It is our present belief that these peaks are the result of similar resonances, and that resonance must be a common occurrence in the flow field of strongly interacting multiple bodies.

Figure 38. Drag coefficient ratios for a 4-vehicle platoon.

Resonance conditions for full-scale vehicles. The resonance condition results in larger drag coefficients than would otherwise occur at short spacing. We would expect similar resonances to occur at a similar spacings for full-scale vehicles for the following reasons. If, as we believe, the resonance is an interaction between t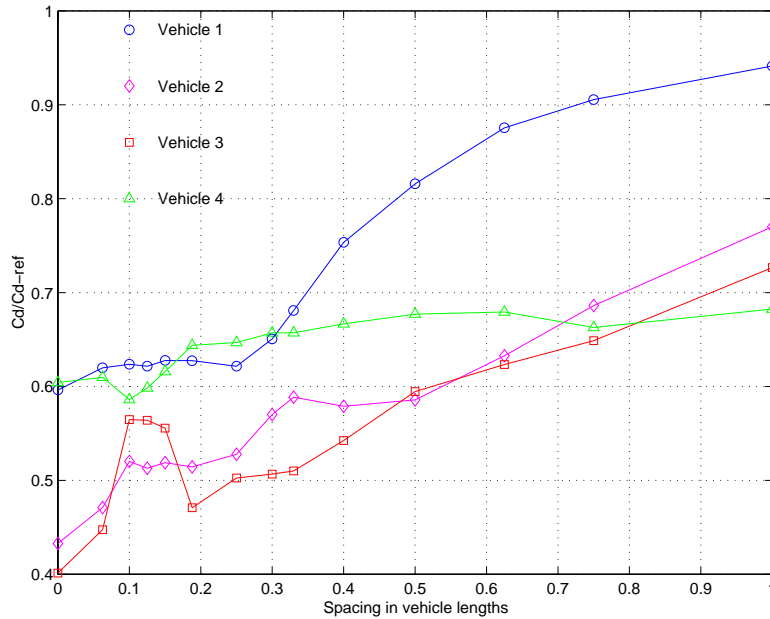he turbulent boundary layer leaving the forward vehicle and the length of the gap between vehicles, the gap, or separation S_G must scale with the boundary layer thickness. That is, referring to figure 37,

$$S_G \approx \lambda \sim \delta$$

For a turbulent boundary layer at the Reynolds numbers relevant here, the boundary layer thickness grows approximately as

$$\delta \sim L^{4/5}$$

where L is the scale of the vehicle. Since 4/5 is almost unity, δ and λ scale approximately with L, and the resonance can be expected to occur at (approximately) the same non-dimensional (scaled) spacings determined by the model tests.

It is interesting to ask how these spacings might apply to the gaps between tractors and trailers and between multiple trailers for full-scale vehicles. Referring again to figure 33, the wind tunnel results show significant increases in drag and severe hysteresis for spacings between 0.05L and 0.12L. The table below considers separately the tractor- trailer gap scaled with a typical tractor length, L_t, and the trailer-trailer gap scaled with a typical trailer length, L_T. From the table, the range of spacings to be avoided for tractor trailer gaps, say approximately 1-2.5 feet, are probably less than the spacings encountered in normal use. However the trailer-trailer gaps of concern fall within the range

2.5-6 feet, and are similar to the gaps now in use. Thus present trailer-trailer gaps may not be optimum, and further work should be done utilizing wind tunnel models which are better geometric representations of tractor and trailers.

Drag rises in wind tunnel tests	0.05 L	-	0.12 L
Tractor-trailer gap, $L_t \cong 6m$ (19.7 feet)	0.3 m (1 foot)	-	0.72 m (2.4 feet)
Trailer-Trailer gap, turnpike double, $L_T \cong 14.6$ m (48 feet)	0.73 m (2.4 feet)	-	1.75 m (5.7 feet)

V. Goals for future research

The present exhaustive set of experiments outline aerodynamic effects which are quantitatively significant (two-fold increase in drag for specific platoon geometries and spacings) and insufficiently understood. Additional experimental information is needed to fully understand and especially to control such phenomena. The following items have been proposed for study over the next two years:

i) Extend the misalignment platoon geometry. Investigation of additional platoon configurations corresponding to the situation when the trailing car closes up on the leading car after the middle car has been totally steered out of the platoon, forming a two-vehicle platoon.

ii) Detailed wind tunnel study of inter-vehicle flow fields. Measurements presented here document forces and yawing moments, but do not provide explanations for how these forces and moments are achieved. In the proposed research task, flowfield data will be acquired using Digital Particle Image Velocimetry, a cutting edge quantitative flow visualization technique. DPIV techniques will provide detailed information in the form of two-dimensional data slices through the inter-vehicle space.

iii) Visualization of flow around full-size vehicles. The similarity between wind tunnel experiments and air flow around full sized vehicles will be documented by performing visualization experiments at El Mirage Dry Lake. Various colored smoke tracers will mark the flowfield between the two vans.

VI. References

Browand, F., Zabat, M., Tokumaru, P., 1997, "Aerodynamic benefits from close-following", Automated Highway Systems, ed. P. Ioannou, Plenum Press, Chapter 12

Gharib, M., Roshko, A., 1987, "The effect of flow oscillations on cavity drag", *J. Fluid Mech.* **177:**501-530

Roshko, A., Koenig, K., 1978, "Interaction effects on the drag of bluff bodies in tandem", In Sovran, G., Morel, T., Mason, W.T., (Ed.): *Aerodynamic Drag Mechanisms of Bluff Bodies and Road Vehicles.* Plenum Press, New York, pp 253-286

Zabat, M., Stabile, N., Frascaroli, S., Browand, F., 1993, "Drag measurements of a platoon of vehicles", PATH Report UCB-ITS-PRR-93-27

Zabat, M., Stabile, N., Frascaroli, S., Browand, F., 1995, The aerodynamic performance of platoons; A final report", PATH Report UCB-ITS-PRR-95-35

Zabat, M., Stabile, N., Frascaroli, S., Browand, F., 1995, "Drag forces experienced by 2, 3 & 4-vehicle platoons at close spacings", SAE Paper No. 950632

Rillings, J. H., "Automated Highways", Scientific American, October 1997, p. 80.

Hong, P., Marcu, B., Browand, F., Tucker, A., 1997, "Drag forces experienced by two, full-scale vehicles at close spacing", SAE paper No. 98B-175, 1998

Appendix A

Databases of experimental measurements

The drag forces, side forces and yawing moments for each member of the three-vehicle platoon are supplied in the form of Matlab binary files as specified in the following table. Each file has an *i,j,k*-type of three-dimensional structure, where *i=1..30, j=1..14, k=1..30,* each value in the file corresponding to a specific platoon configuration. The configuration geometry is specified in the three position files *vsx1.mat*, *vsy2.mat* and *vsx3.mat* (see table). Thus, for example, when one needs the drag value corresponding to a configuration geometry corresponding to a certain separation between the lead and middle car *sx1*, a certain missalignment for the middle car *sy2*, and certain separation between the middle and the trail car *sx3*, one should identify which *i* position in the *vsx1.mat* file corresponds to the desired *sx1* value, which *j* position in the *vsy2.mat* file corresponds to the desired *sy2* value, and which *k* position in the *vsx3.mat* file corresponds to the desired *sx3* value, then extract the drag for the leading car from the *vcd1.mat* file at the identified *i,j,k* position, and so on. Forces and yawing moment values are in non-dimensional ratio forms (see report), while the separation and missalignment values are expressed in vehicle lengths and vehicle widths respectively.

File No	File name	File Description.
1	vcd1.mat	leading vehicle drag force values
2	vcd2.mat	middle vehicle drag force values
3	vcd3.mat	trailing vehicle drag force values
4	vcs1.mat	leading vehicle side forces
5	vcs2.mat	middle vehicle side forces
6	vcs3.mat	trailing vehicle side forces
7	vcy1.mat	leading vehicle yawing moment
8	vcy2.mat	middle vehicle yawing moment
9	vcy3.mat	trailing vehicle yawing moment
10	vsx1.mat	separation between leading and middle vehicle
11	vsy2.mat	lateral misalignment of the middle vehicle
12	vsx3.mat	separation between the middle and trailing vehicle